

---

## Reduced models of the cardiovascular system

Joaquim Peiró, Alessandro Veneziani

Due to the large number of vessels involved and the multitude of different length scales required to accurately represent the flow in the various regions of the cardiovascular system, simulations of the flow of blood in the system based on full 3D models (see Chapters 2 and 3) are beyond the capability of current computers and they will be for years to come. Moreover, the huge amount of data that would be generated by such simulations is costly to process and of difficult clinical interpretation.

However, it is possible to devise simplified models exploiting specific features of blood flow, such as the basically cylindrical morphology of the vessels. Even though these models are highly simplified with respect to the local dynamics, they can provide reliable numerical results at a low computational cost. Interpretation is much straightforward, thus making them ideal as an everyday tool for use in clinical practice.

Moreover, these models are well-suited for describing systemic dynamics such as *feedback mechanisms* that play an important role in the correct working of the vascular system. These dynamics typically involve mechanical and biochemical phenomena that can be hardly described in terms of complete 3D models.

In this chapter, we address simplified models and in particular we consider:

1. one-dimensional (1D) models in which the space dependence is reduced only to the axial coordinate;
2. lumped parameter (or 0D) models, where the space dependence is discretised, by splitting the cardiovascular system into a set of compartments. The associated mathematical model is typically based on differential algebraic equations (DAE), often represented in terms of hydraulic or electric networks.

It is worth mentioning that studies on one-dimensional models of blood flow were first presented by Leonhard Euler in his seminal article entitled *Pro principa motu sanguinis per arterias determinando* [139]. In spite of the simplifying assumptions behind these models, they are very useful and

many of their analytical and numerical aspects still deserve further investigation<sup>1</sup>.

## 10.1 One-dimensional (1D) models

There are several ways of deriving a 1D model of an incompressible fluid flowing in a compliant pipe. One could start from the incompressible Navier-Stokes equations and perform an asymptotic analysis by assuming that the radius of the vessel,  $R_0$ , is small compared to its length  $l$ , i.e.  $\frac{R_0}{L} \ll 1$ , that will permit us to simplify the governing equations by discarding the higher order terms in  $\frac{R_0}{L}$ , as proposed in [25]. Alternatively, the 1D model could be derived by assuming cylindrical symmetry and integrating the Navier-Stokes equations on a generic section as described in [364].

Here we will follow the approach advocated and described in [238,239] and derive the governing equations from conservation principles. This approach is more general and it does not require any simplifying assumptions concerning the geometry of the vessel section.

### 10.1.1 Derivation of the governing equations

We consider a simple compliant tube, illustrated in Fig. 10.1, as a model of the artery. We assume that the axis of the vessel is rectilinear and coincides with the  $x$  axis. The starting point for the derivation of the one-dimensional governing equations is Reynolds' transport theorem for an arbitrary control volume  $V_t$  with boundary  $\partial V_t$  and outer normal  $\mathbf{n}$ . A formal derivation of this formula can be found in Chapter 2 of this book and in [401]. It states that, for a continuous function  $f = f(t, \mathbf{x})$ , we have

$$\frac{d}{dt} \int_{V_t} f dV = \int_{V_t} \frac{\partial f}{\partial t} dV + \int_{\partial V_t} f \mathbf{u}_b \cdot \mathbf{n} d\sigma, \quad (10.1)$$

where  $\mathbf{x}$  stands for  $(x, y, z)$  and  $\mathbf{u}_b$  is the velocity of the boundary of volume  $V_t$ . This is composed of the arterial wall  $\partial V_{t,w}$  and the two end sections  $S_1$  and  $S_2$ , that are assumed normal to the axis. On  $S_1$  and  $S_2$  the normal component of  $\mathbf{u}_b$  is 0, while on  $\partial V_{t,w}$  velocity  $\mathbf{u}_b$  does coincide with the velocity  $\mathbf{u}_w$  of the arterial wall, so that

$$\int_{\partial V_t} f \mathbf{u}_b \cdot \mathbf{n} d\sigma = \int_{\partial V_{t,w}} f \mathbf{u}_w \cdot \mathbf{n} d\sigma. \quad (10.2)$$

---

<sup>1</sup> "Thus in explaining the motion of the blood, we come up against the same insuperable difficulties which clearly prevent us from more accurately investigating all the works of the Creator; wherein we ought constantly to admire and to venerate much more the highest wisdom conjoined with omnipotence since truly not even the greatest human ingenuity avails to understand and explain the true structure of the slightest micro-organism", L. Euler [139].

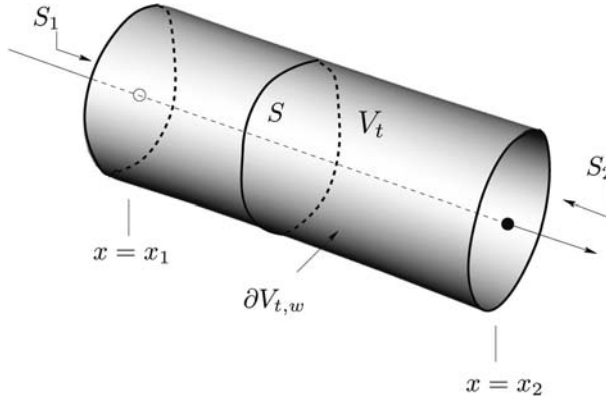


**Fig. 10.1.** Notation used to describe a simple compliant tube

Here  $\mathbf{u}_w$  is taken to be different of the fluid velocity  $\mathbf{u} = (u_1, u_2, u_3)$  to allow for the presence of a permeable lumen. The relative velocity between the arterial wall and the fluid at the lumen is given by

$$\mathbf{w} = \mathbf{u}_w - \mathbf{u}.$$

To obtain the one-dimensional form of the conservation laws, we consider area-averaged values of the relevant variables. The area-averaged value of  $f$  is denoted by  $\bar{f}$  and given by

$$\bar{f} = \frac{1}{A} \int_S f \, d\sigma, \tag{10.3}$$

where  $A = A(x, t) = \int_S d\sigma$  is the area of the cross section  $S$ . Using this notation, we write a volume integral as

$$\int_{V_t} f \, dV = \int_{x_1}^{x_2} \left[ \int_S f \, d\sigma \right] dx = \int_{x_1}^{x_2} A \bar{f} \, dx, \tag{10.4}$$

where  $x_1$  and  $x_2$  ( $x_2 > x_1$ ) are the  $x$ -coordinates of the cross sections  $S_1$  and  $S_2$ .

Given that  $x_1$  and  $x_2$  are independent of time, the left-hand side term of equation (10.1) can be written as

$$\frac{d}{dt} \int_{V_t} f \, dV = \int_{x_1}^{x_2} \frac{\partial}{\partial t} (A \bar{f}) \, dx. \tag{10.5}$$

The presence of a permeable wall makes the evaluation of the second term of the right-hand side of equation (10.1) more involved. After (10.2), this term is calculated as

$$\int_{\partial V_{t,w}} f \mathbf{u}_w \cdot \mathbf{n} \, d\sigma = \int_{\partial V_{t,w}} f \mathbf{w} \cdot \mathbf{n} \, d\sigma + \int_{\partial V_{t,w}} f \mathbf{u} \cdot \mathbf{n} \, d\sigma.$$

Observe that

$$\int_{\partial V_{t,w}} f\mathbf{u} \cdot \mathbf{n} \, d\sigma = \int_{\partial V_t} f\mathbf{u} \cdot \mathbf{n} \, d\sigma - \int_{S_1} f\mathbf{u} \cdot \mathbf{n} \, d\sigma - \int_{S_2} f\mathbf{u} \cdot \mathbf{n} \, d\sigma = \int_{\partial V_t} f\mathbf{u} \cdot \mathbf{n} \, d\sigma + \int_{S_1} fu_1 \, d\sigma - \int_{S_2} fu_1 \, d\sigma,$$

where  $u_1$  is the  $x$ -component of the velocity  $\mathbf{u}$ . Thanks to the Gauss' theorem, we have

$$\int_{\partial V_{t,w}} f\mathbf{u} \cdot \mathbf{n} \, d\sigma = \int_{V_t} \nabla \cdot (f\mathbf{u}) \, dV + \int_{S_1} fu_1 \, d\sigma - \int_{S_2} fu_1 \, d\sigma,$$

so that using area-averaged quantities, we finally obtain

$$\int_{\partial V_{t,w}} f\mathbf{u}_w \cdot \mathbf{n} \, d\sigma = \int_{\partial V_{t,w}} f\mathbf{w} \cdot \mathbf{n} \, d\sigma - \int_{x_1}^{x_2} \frac{\partial}{\partial x} [A(\overline{fu_1})] \, dx + \int_{V_t} \nabla \cdot (f\mathbf{u}) \, dV, \tag{10.6}$$

Finally, including the expressions (10.5) and (10.6) into equation (10.1) leads to

$$\int_{x_1}^{x_2} \frac{\partial}{\partial t} (A\bar{f}) \, dx = \int_{x_1}^{x_2} \left( \int_S \frac{\partial f}{\partial t} \, d\sigma \right) \, dx + \int_{x_1}^{x_2} \left( \int_{\partial S} f\mathbf{w} \cdot \mathbf{n} \, d\gamma \right) \, dx - \int_{x_1}^{x_2} \frac{\partial}{\partial x} [A(\overline{fu_1})] \, dx + \int_{x_1}^{x_2} \left( \int_S \nabla \cdot (f\mathbf{u}) \, d\sigma \right) \, dx,$$

and, given that this is true for any values of the coordinates of the end sections  $x_1$  and  $x_2$ , the final form of the one-dimensional transport theorem for a generic variable  $f$  is

$$\frac{\partial}{\partial t} (A\bar{f}) + \frac{\partial}{\partial x} [A(\overline{fu_1})] = \int_S \left[ \frac{\partial f}{\partial t} + \nabla \cdot (f\mathbf{u}) \right] \, d\sigma + \int_{\partial S} f\mathbf{w} \cdot \mathbf{n} \, d\gamma. \tag{10.7}$$

This formula is general and applicable to both compressible and incompressible fluids. Now we will proceed to derive the governing equations by invoking the principles of conservation of mass and balance of momentum.

**Conservation of mass**

The equation representing the conservation of mass in the flexible tube is obtained by taking  $f = 1$  in equation (10.7). If we further assume that the fluid is incompressible, i.e.  $\nabla \cdot \mathbf{u} = 0$ , we get

$$\frac{\partial A}{\partial t} + \frac{\partial}{\partial x} (A\bar{u}_1) = \int_{\partial S} \mathbf{w} \cdot \mathbf{n} \, d\gamma, \tag{10.8}$$

where the term in the right-hand side could be interpreted as a volumetric outflow per unit length and unit time.

### Balance of momentum

Here we take  $f = u_1$  in the area-averaged Reynolds' transport expression (10.7), and assume again that the fluid is incompressible, to obtain

$$\frac{\partial}{\partial t}(A\bar{u}_1) + \frac{\partial}{\partial x}(A\bar{u}_1^2) = \int_S \left[ \frac{\partial u_1}{\partial t} + \mathbf{u} \cdot \nabla u_1 \right] d\sigma + \int_{\partial S} u_1 \mathbf{w} \cdot \mathbf{n} d\gamma, \quad (10.9)$$

which we now write as

$$\frac{\partial}{\partial t}(A\bar{u}_1) + \frac{\partial}{\partial x}(A\bar{u}_1^2) = \int_S \frac{Du_1}{Dt} d\sigma + \int_{\partial S} u_1 \mathbf{w} \cdot \mathbf{n} d\gamma, \quad (10.10)$$

where  $\frac{D}{Dt} = \frac{\partial}{\partial t} + \mathbf{u} \cdot \nabla$  denotes the material derivative (see Chapter 3). To calculate the first term on the right-hand side of equation (10.10) we use the balance of momentum derived in Chapter 3 for the control volume  $V_t$  in the form

$$\int_{V_t} \frac{D}{Dt}(\rho \mathbf{u}) dV = \int_{V_t} \rho \mathbf{f}^b dV + \int_{\partial V_t} \mathbf{T} \mathbf{n} d\sigma, \quad (10.11)$$

where  $\mathbf{f}^b$  represents the body force per unit volume and  $\mathbf{T}$  is the Cauchy stress tensor. Assuming that the density  $\rho$  is constant and using the divergence theorem, the balance of momentum equation (10.11) is written as

$$\int_{V_t} \frac{D\mathbf{u}}{Dt} dV = \int_{V_t} \mathbf{f}^b dV + \frac{1}{\rho} \int_{V_t} \nabla \cdot \mathbf{T} dV. \quad (10.12)$$

Now, invoking the constitutive equation for the fluid, we could write the stress tensor  $\mathbf{T}$  as

$$\mathbf{T} = -p\mathbf{I} + \mathbf{D}, \quad (10.13)$$

where  $p$  denotes the pressure,  $\mathbf{I}$  is the identity tensor, and  $\mathbf{D}$  represents the tensor of deviatoric stresses due to the viscosity of the fluid. Setting  $\nabla \cdot \mathbf{D} = \mathbf{d}$  we also write

$$\nabla \cdot \mathbf{T} = -\nabla p + \nabla \cdot \mathbf{D} = -\nabla p + \mathbf{d},$$

and, therefore, equation (10.12) as

$$\int_{x_1}^{x_2} \left( \int_S \frac{D\mathbf{u}}{Dt} d\sigma \right) dx = \int_{x_1}^{x_2} \left( \int_S \left[ \mathbf{f}^b + \frac{1}{\rho} (-\nabla p + \mathbf{d}) \right] d\sigma \right) dx. \quad (10.14)$$

Since  $x_1$  and  $x_2$  can be arbitrarily chosen, the integrands in the left and right-hand sides of equation (10.14) must be equal, therefore we could write the  $x$ -component of this equation as

$$\int_S \frac{Du_1}{Dt} d\sigma = \int_S \left[ f_1^b + \frac{1}{\rho} \left( -\frac{\partial p}{\partial x} + d_1 \right) \right] d\sigma, \quad (10.15)$$

where  $d_1$  is the  $x$ -component of  $\mathbf{d}$ . Substituting this expression in equation (10.10) gives

$$\frac{\partial}{\partial t}(A\bar{u}_1) + \frac{\partial}{\partial x}(A\bar{u}_1^2) = \int_S \left[ f_1^b + \frac{1}{\rho} \left( -\frac{\partial p}{\partial x} + d_1 \right) \right] d\sigma + \int_{\partial S} u_1 \mathbf{w} \cdot \mathbf{n} d\sigma, \quad (10.16)$$

which can be expressed using area-averaged values as

$$\frac{\partial}{\partial t}(A\bar{u}_1) + \frac{\partial}{\partial x}(A\bar{u}_1^2) = \frac{A}{\rho} \left( \rho \bar{f}_1^b - \frac{\partial \bar{p}}{\partial x} + \bar{d}_1 \right) + \int_{\partial S} u_1 \mathbf{w} \cdot \mathbf{n} d\sigma. \quad (10.17)$$

The term  $\bar{u}_1^2$  in this equation is handled by defining a momentum-flux correction coefficient  $\alpha$  (sometimes called the Coriolis coefficient), which is a function of the velocity profile, as

$$\bar{u}_1^2 = \frac{1}{A} \int_S u_1^2 d\sigma = \alpha \bar{u}_1^2. \quad (10.18)$$

For a flat profile we have  $\alpha = 1$  and for a parabolic flow  $\alpha = 4/3$ .

The term representing the viscous forces  $\bar{d}_1$  is taken to be a linear function of the area-averaged velocity  $\bar{u}_1$  of the form

$$\frac{A}{\rho} \bar{d}_1 = -K_R \bar{u}_1, \quad (10.19)$$

where  $K_R$  is a strictly positive quantity which represents the viscous resistance of the flow per unit length of tube. It is worth observing that for a proper definition of the coefficient, (10.19) is fulfilled by the Poiseuille flow (see Chapter. 5). The final form of the balance of momentum equation is

$$\frac{\partial}{\partial t}(A\bar{u}_1) + \frac{\partial}{\partial x}(\alpha \bar{u}_1^2) = A \bar{f}_1^b - \frac{A}{\rho} \left( \frac{\partial \bar{p}}{\partial x} \right) - K_R \bar{u}_1 + \int_{\partial S} u_1 \mathbf{w} \cdot \mathbf{n} d\sigma. \quad (10.20)$$

The unknowns in the system given by (10.8) and (10.20) are  $p$ ,  $A$  and  $\bar{u}_1$ . Their number exceeds the number of equations and a common way to close the system is to explicitly provide a relationship between the pressure of the vessel  $p$  and the vessel area  $A$ . This relation will be derived from the models introduced in Chapter 3, in particular the algebraic relation (3.94).

### Simplified models of wall mechanics

By assuming *static equilibrium* in the radial direction of a cylindrical tube, from one-dimensional models of wall mechanics described in Section 3.4.4 one can derive an algebraic relationship of the form

$$p = P_{ext} + \beta \left( \sqrt{A} - \sqrt{A_0} \right), \quad (10.21)$$

where

$$\beta = \frac{\sqrt{\pi}h_0E}{(1 - \nu^2)A_0}. \tag{10.22}$$

Here  $h_0$  and  $A_0 = A_0(x)$  denote the vessel thickness and sectional area, respectively, at the equilibrium state  $(p, Q) = (P_{ext}, 0)$ ,  $E = E(x)$  is the Young modulus,  $P_{ext}$  is the external pressure, assumed constant, and  $\nu$  is the Poisson ratio. This ratio is typically taken to be  $\nu = 1/2$  since biological tissue is practically incompressible. More generally, we may have

$$p = P_{ext} + \Phi(A; A_0, \beta), \tag{10.23}$$

being  $\Phi$  a suitable function of the vessel section  $A$  and of the reference area  $A_0$  as well as some mechanical parameter  $\beta$ . The main properties of  $\Phi$  are

$$\frac{\partial \Phi}{\partial A} > 0, \quad \Phi(A_0; A_0, \beta) = 0,$$

for all allowable values of  $A$ ,  $A_0$  and  $\beta$ .

The algebraic relation (10.23), and in particular (10.21), assumes that the wall is instantaneously in equilibrium with the pressure forces acting on it.

Wall inertia and viscoelasticity can be included, yielding a differential pressure law. For instance, moving from (3.91) we may write

$$p - P_{ext} = \gamma_0 \frac{\partial^2 \eta}{\partial t^2} + \gamma_1 \frac{\partial \eta}{\partial t} + \Phi(A; A_0, \beta), \tag{10.24}$$

where  $\gamma_0 = \rho_w h_0$ ,  $\gamma_1 = \frac{\gamma}{r_0^2}$  and the last term is the elastic response, modelled through equation (10.21). Here  $\gamma$  is the same viscoelasticity coefficient of (3.93) and  $\eta$  is the wall position. In the following, we indicate by  $\dot{A}$  and  $\ddot{A}$  the first and second time derivative of  $A$ . By assuming a circular profile  $A = \pi\eta^2$ , thus

$$\frac{\partial \eta}{\partial t} = \frac{1}{2\sqrt{\pi A}} \dot{A}, \quad \frac{\partial^2 \eta}{\partial t^2} = \pi^{-\frac{1}{2}} \left( \frac{1}{2\sqrt{A}} \ddot{A} - \frac{1}{4\sqrt{A^3}} \dot{A}^2 \right). \tag{10.25}$$

Using these relations into (10.24) we obtain an equation that links the pressure also to the time derivatives of  $A$ , which we write in all generality as

$$p - P_{ext} = \tilde{\Phi}_E(A, \dot{A}, \ddot{A}; A_0) + \Phi(A; A_0, \beta),$$

where  $\tilde{\Phi}_E$  is a non-linear function which derives from the treatment of the terms containing the time derivative of  $\eta$ . Since it may be assumed that the contribution to the pressure is in fact dominated by the term  $\Phi$ , we will simplify this relationship by linearizing  $\tilde{\Phi}_E$  around the state  $A = A_0$ ,  $\dot{A} = \ddot{A} = 0$ . By so doing, after some simple algebraic manipulations, one finds

$$p - P_{ext} = \frac{\gamma_0}{2\sqrt{\pi A_0}} \ddot{A} + \frac{\gamma_1}{2\sqrt{\pi A_0}} \dot{A} + \Phi(A; A_0, \beta). \tag{10.26}$$

Replacing this expression for the pressure in the momentum equation requires to compute the term

$$\frac{A}{\rho} \frac{\partial p}{\partial x} = \frac{\gamma_0 A}{2\rho\sqrt{\pi A_0}} \frac{\partial^3 A}{\partial x \partial t^2} + \frac{\gamma_1 A}{2\rho\sqrt{\pi A_0}} \frac{\partial^2 A}{\partial x \partial t} + \frac{A}{\rho} \frac{\partial \Phi}{\partial x}.$$

Wall inertia introduces a *dispersive* term into the momentum equation, while the viscoelasticity has a *diffusive* effect. This has implications on the numerical solution.

In the following we will consider only relation (10.21) to discuss the properties of the resulting scheme and its numerical formulation. Most of the discussion, however, can be extended to any model based on a pressure-area relation of the form (10.23).

### 10.1.2 Different formulations of the governing equations

In what follows, we will assume that the lumen is impermeable ( $\mathbf{w} \cdot \mathbf{n} = 0$ ), that body forces are negligible ( $\bar{f}_1^b = 0$ ), and we will also simplify the notation by denoting the area-averaged axial velocity by  $u$  instead of  $\bar{u}_1$  and using  $p$  instead of  $\bar{p}$ . Defining the mass flux across a section as  $Q = Au = \int_S u_1 d\sigma$ , the equations (10.8) and (10.20) now read

$$\begin{aligned} \frac{\partial A}{\partial t} + \frac{\partial Q}{\partial x} &= 0, \\ \frac{\partial Q}{\partial t} + \frac{\partial}{\partial x} \left( \alpha \frac{Q^2}{A} \right) + \frac{A}{\rho} \left( \frac{\partial p}{\partial x} \right) + K_R \frac{Q}{A} &= 0. \end{aligned} \tag{10.27}$$

The couple  $(A, Q)$  will be referred to as *conserved variable* since they stem naturally from the application of conservation principles.

The system of equations (10.27) can be expressed alternatively in terms of the variables  $(A, u)$ . By simple manipulations one gets

$$\begin{aligned} \frac{\partial A}{\partial t} + \frac{\partial Au}{\partial x} &= 0, \\ \frac{\partial u}{\partial t} + (2\alpha - 1)u \frac{\partial u}{\partial x} + (\alpha - 1)u^2 \frac{\partial A}{\partial x} + \frac{1}{\rho} \frac{\partial p}{\partial x} + K_R \frac{u}{A} &= 0. \end{aligned} \tag{10.28}$$

Both systems (10.27) and (10.28) may be written in *conservation form*. Let us assume for instance that the wall mechanics is described by the algebraic pressure-wall relationship (10.21).

For the system  $(A, Q)$  we have

$$\frac{\partial \mathbf{Q}}{\partial t} + \frac{\partial \mathbf{G}}{\partial x}(\mathbf{Q}) = \mathbf{B}(\mathbf{Q}), \tag{10.29}$$

with

$$\mathbf{Q} = \begin{bmatrix} A \\ Q \end{bmatrix}, \quad \mathbf{G} = \left[ \alpha \frac{Q^2}{A} + \int_{A_0}^A \frac{a}{\varphi} \frac{\partial \rho}{\partial a} da \right] \quad \text{and}$$

$$\mathbf{B} = \begin{bmatrix} 0 \\ -K_R \frac{Q}{A} + \frac{A}{\varphi} \left( \frac{\partial \rho}{\partial A_0} \frac{\partial A_0}{\partial x} + \frac{\partial \rho}{\partial \beta} \frac{\partial \beta}{\partial x} \right) \end{bmatrix}. \quad (10.30)$$

For the  $(A, u)$  system, if for the sake of simplicity we assume  $\alpha = 1$ , we have

$$\frac{\partial \mathbf{U}}{\partial t} + \frac{\partial \mathbf{F}}{\partial x}(\mathbf{U}) = \mathbf{S}(\mathbf{U}), \quad (10.31)$$

with

$$\mathbf{U} = \begin{bmatrix} A \\ u \end{bmatrix}, \quad \mathbf{F} = \begin{bmatrix} Au \\ p_t \end{bmatrix} \quad \text{and} \quad \mathbf{S} = \begin{bmatrix} 0 \\ -K_R \frac{u}{A} \end{bmatrix}. \quad (10.32)$$

Here

$$p_t = \frac{u^2}{2} + \frac{p}{\rho}, \quad (10.33)$$

denotes the *total pressure* (scaled by the constant density).

In the case  $\alpha = 1$  the two weak forms are equivalent for smooth solutions, in particular when  $A$  and  $Q$  are  $C^1$  continuous functions with respect to both arguments and  $A$  is strictly positive. Nevertheless, the assumption  $\alpha = 1$  is quite realistic in the problems at hand since the velocity profile is in fact almost flat (see Chapter 1 and [350]) and the solutions within each of the approaches presented in this chapter will be sufficiently smooth to favour the use of the  $(A, u)$  system which has a simpler structure.

The  $(A, u)$  and the  $(A, Q)$  systems given respectively by equations (10.28) and (10.27), together with the algebraic pressure-area relationship (10.21), will be starting points of the numerical schemes discussed in Section 10.1.8.

**Remark 10.1.1** *Even though the values of the coefficients  $\alpha$ ,  $K_R$  and  $\beta$  are fixed a priori once we make assumptions on the velocity profile and on the wall mechanics, it is also possible to interpret them as parameters of the model that can be obtained by fitting the results of the 1D model to available in vivo or 3D computational data as proposed in [314].*

### 10.1.3 1D models for blood solutes

The relevance of the dynamics of blood solutes and its coupling with haemodynamics have been extensively addressed in Chapter 7. Since the dynamics of these solutes is relevant for regulatory mechanisms that involve large parts of the cardiovascular system and are fundamental for its proper working (see Section 10.2.4), it is worth to devise simple models also for biochemical dynamics (see [108]). As done in Section 7.1 of Chapter 7, we assume that the

solute concentration  $c(\mathbf{x}, t)$  satisfies a (linear) advection-diffusion equation in the form

$$\frac{\partial c}{\partial t} - \mu_s \Delta c + \mathbf{u} \cdot \nabla c = 0,$$

in the domain  $\Omega_t$  ( $\mathbf{u}$  is the blood velocity), together with a suitable initial condition  $c(\mathbf{x}, 0) = c_0(\mathbf{x})$ . We assume that a Robin condition  $\nu \nabla c \cdot \mathbf{n} = \chi(c_{ext} - c)$  is given on the vascular wall. Here coefficient  $\chi$  denotes the *permeability*. For the sake of simplicity, we will assume that  $c_{ext} = 0$ .

By using area-averaged quantities, in a way similar to the one adopted for the Navier-Stokes equations, and setting  $\Gamma = A\bar{c}$ , it is possible to obtain the following 1D solute equation

$$\frac{\partial \Gamma}{\partial t} + \frac{\partial}{\partial x} \left( \omega \frac{\Gamma Q}{A} \right) + K_c \frac{\Gamma}{A} = 0, \quad x_1 < x < x_2, \quad (10.34)$$

to be completed with suitable boundary conditions. Coefficient  $\omega$  depends on the axial velocity and concentration profiles (similar to the Coriolis coefficient) and  $K_c$  is a coefficient depending on the viscosity  $\mu_s$  and the permeability  $\chi$ . Equation (10.34) can be therefore coupled to (10.27) for a complete model of the blood and solutes dynamics. For an extensive analysis see [108].

### 10.1.4 Characteristic variables

Considering the pressure-area relationship (10.21) and assuming that  $\beta = \beta(x)$  and  $A_0 = A_0(x)$  we recall that applying the chain rule we obtain

$$\frac{\partial p}{\partial x} = \frac{\partial p}{\partial A} \frac{\partial A}{\partial x} + \frac{\partial p}{\partial \beta} \frac{\partial \beta}{\partial x} + \frac{\partial p}{\partial A_0} \frac{\partial A_0}{\partial x},$$

where

$$\frac{\partial p}{\partial A} = \frac{\beta}{2\sqrt{A}}.$$

System (10.28) can therefore be written inquasi-linear form as

$$\frac{\partial \mathbf{U}}{\partial t} + \mathbf{H} \frac{\partial \mathbf{U}}{\partial x} = \mathbf{f}(\mathbf{U}), \quad (10.35)$$

or, more explicitly

$$\begin{bmatrix} A \\ u \end{bmatrix}_t + \begin{bmatrix} u & A \\ c^2/A & u \end{bmatrix} \begin{bmatrix} A \\ u \end{bmatrix}_x = \begin{bmatrix} 0 \\ f \end{bmatrix},$$

where

$$c^2 = \frac{A}{\rho} \frac{\partial p}{\partial A} = \frac{\beta\sqrt{A}}{2\rho} \quad \text{and} \quad f = \frac{1}{\rho} \left[ K_R u - \frac{\partial p}{\partial \beta} \frac{\partial \beta}{\partial x} + \frac{\partial p}{\partial A_0} \frac{\partial A_0}{\partial x} \right].$$

Under the assumption that  $A > 0$ , which is indeed a necessary condition to have a physically relevant solution, the matrix  $\mathbf{H}$  has two real eigenvalues  $\lambda_{1,2} = u \pm c$  and the corresponding left eigenmatrix  $\mathbf{L}$  is

$$\mathbf{L} = \begin{bmatrix} \mathbf{l}_1^T \\ \mathbf{l}_2^T \end{bmatrix} = \begin{bmatrix} \frac{c}{A} & 1 \\ -\frac{c}{A} & 1 \end{bmatrix}, \quad (10.36)$$

where  $\mathbf{l}_i$  indicates the  $i$ -th left eigenvector such that  $\mathbf{l}_i^T \mathbf{H} = \lambda_i \mathbf{l}_i^T$ . We will also indicate by  $\mathbf{R} = [\mathbf{r}_1 \ \mathbf{r}_2] = \mathbf{L}^{-1}$  the corresponding right eigenmatrix. For the typical values of velocity, vessel area and elastic parameter  $\beta$  encountered in arteries under physiological conditions, we have that  $\lambda_1 > 0$  and  $\lambda_2 < 0$ . Therefore our system is *strictly hyperbolic* and *subcritical* (see [277] for these definitions).

The characteristic variables can be determined by integrating the differential system  $\partial_U \mathbf{W} = \mathbf{L}$ . It may be shown that this is possible for our problem and that the two characteristic variables are

$$W_1 = u + 4c = u + 4A^{1/4} \sqrt{\frac{\beta}{2\rho}}, \quad (10.37)$$

$$W_2 = u - 4c = u - 4A^{1/4} \sqrt{\frac{\beta}{2\rho}}. \quad (10.38)$$

Since  $\beta > 0$ , we may write, as previously reported in [160], the variables  $(A, u)$  in terms of  $(W_1, W_2)$  as

$$A = \left[ \frac{(W_1 - W_2)}{4} \right]^4 \left( \frac{\rho}{2\beta} \right)^2 \quad u = \frac{(W_1 + W_2)}{2}. \quad (10.39)$$

In the case where  $f = 0$  equations (10.35) can be transformed in a decoupled system of equations for the characteristic variables, which component-wise reads

$$\begin{aligned} \frac{\partial W_1}{\partial t} + \lambda_1 \frac{\partial W_1}{\partial x} &= 0, \\ \frac{\partial W_2}{\partial t} + \lambda_2 \frac{\partial W_2}{\partial x} &= 0. \end{aligned} \quad (10.40)$$

We recall that the expression of the characteristic variables, as well as that of the  $\lambda_i$  are independent from the choice of the governing variables of our problem. This is not the case for  $\mathbf{L}$  and  $\mathbf{R}$ .

**Remark 10.1.2** Smoothness of the solution. *We recall some of the main results regarding the hyperbolic system at hand. It has been shown in [7, 524] that, using a pressure-area relationship of the form*

$$p - P_{ext} = G_0 \left[ \left( \frac{A}{A_0} \right)^{\frac{\alpha}{2}} - 1 \right],$$

where  $\delta > 1$  and  $G_0$  is a constant elasticity parameter, and under some reasonable conditions on the smoothness of boundary and initial data, the solution of system (10.27) remains smooth. Two critical assumptions to reach this conclusion are the pulsatility of the inflow data and a bound on the length of the tube; both are verified for physiological flow in the human arterial tree. In the same work it is shown that, if the solution is smooth and the initial and boundary data are such that  $A > 0$ ,  $A$  remains strictly positive for all times. In [155] an energy inequality was derived which bounds a measure of the energy of the hyperbolic system in terms of the initial and boundary data. Furthermore, in the same work it has been found that the quantity

$$s = \frac{1}{2}\rho Au^2 + \int_{A_0}^A (p - P_{ext})dA,$$

is an entropy function for the system with associated flux equal to  $\mathbf{F}_s = \mathbf{Q} p_t$ .

### 10.1.5 Boundary conditions

The characteristic analysis and the fact that for physiological conditions the flow is subcritical (i.e.  $\lambda_1 > 0$  and  $\lambda_2 < 0$ ) leads us to the conclusion that only one boundary condition has to be imposed at each end of the tube. Different type of boundary conditions may be envisaged. For the sake of simplicity let us focus on the boundary  $x = x_1$ , the arguments being easily extended to the other boundary point. Here, the sign of the eigenvalues tell us that  $W_1$  is associated to the characteristics entering the domain, while  $W_2$  to the one exiting. Let here  $\mathbf{U} = \mathbf{U}(t)$  indicate the vector of primitive variables at the boundary point  $x = x_1$ , either in the form  $(A, Q)$  or  $(A, u)$ , depending on the choice of the adopted differential model. A boundary condition may take the general form

$$\varphi(\mathbf{U}(t)) = g(t), \quad \text{for } t > 0, \tag{10.41}$$

being  $\varphi$  a  $C^1$  function defined for all allowed values of  $\mathbf{U}$  and  $g$  a given function of time. Not all the choices are possible, indeed we require that the boundary be not characteristic, a condition that in our case is satisfied if for all admissible  $\mathbf{U}$

$$\mathbf{r}_1^T(\mathbf{U}) \frac{\partial \varphi(\mathbf{U})}{\partial \mathbf{U}} \neq 0, \tag{10.42}$$

where  $\mathbf{r}_1$  is the right eigenvector associated to  $\lambda_1$ .

In practice we are interested in specific types of boundary conditions, some of which are detailed in the following paragraphs.

### Non-reflecting boundary conditions

Non-reflecting boundary conditions are those that allow the simple wave associated with the characteristics exiting the domain to leave without spurious reflections. Typically those conditions are expressed in terms of the characteristic variables. Again, let us focus on one of the two boundary points, here we

choose  $x = x_2$ , and on problem (10.31), the modifications for system (10.29) and for the other vessel end being immediate.

Following [502] and [216] non-reflecting boundary conditions at  $x = x_2$  are provided as

$$\mathbf{l}_2^T \left[ \frac{\partial \mathbf{U}}{\partial t} - \mathbf{S}(\mathbf{U}) \right]_{x=x_2} = 0,$$

which indeed is equivalent to state that at  $x = x_2$

$$\frac{dW_2(t)}{dt} = \mathbf{l}_2^T \mathbf{S}(W_2(\mathbf{U}(t))), \quad \text{for } t > 0.$$

Here we have set  $W_2(t) = W_2(x_2, t)$ ,  $\mathbf{U}(t) = \mathbf{U}(x_2, t)$  and we have recalled that the characteristic variable may in our case be expressed in function of the primitive variables of our differential problem. Being basically a condition on the incoming characteristics, relation (10.42) is satisfied. Numerically, this ordinary differential equation will be discretised in time, for instance the computation of  $W_2$  in  $x = x_2$  and at time  $t^{n+1} = t^n + \Delta t$  may be carried out as

$$W_2^{n+1} = W_2^n + \Delta t \mathbf{l}_2^T \mathbf{S}^n,$$

where  $\mathbf{l}_2$  and  $\mathbf{S}$  are computed from the solution at time  $t^n$ .

For the notable case  $\mathbf{S}(\mathbf{U}) = \mathbf{0}$ , or  $\mathbf{B}(\mathbf{Q}) = \mathbf{0}$  if we use (10.29), we have  $W_2 = \text{const}$ , that is a constant incoming characteristic variable.

In our case a condition of this type may be convenient at the distal section (typically  $x = x_2$ ) whenever one can neglect possible contributions of waves coming from the distal circulation, while at the proximal section ( $x = x_1$ ) we would like to prescribe some given values of pressure or flux data coming either from measurement or other models. When the peripheral circulation is taken into account, we need specific models for the terminal vessels that will be discussed later.

### Proximal conditions

It is immediate to verify that the prescription of either a flux  $Q$  (or velocity  $u$ ) or area  $A$  at  $x = x_1$  is allowable. For instance, we may impose

$$A(x_1, t) = g(t), \quad t > 0,$$

where  $g(t)$  is a known function obtained, for instance, from the knowledge of the pressure time variation at  $x = x_1$ . This type of condition is clearly of reflective type and the simple wave associated to the outgoing characteristic ( $W_2$  in this case) may be partly reflected back into the computational domain. Yet, in the case where the measurements are accurate enough, this reflection is indeed a physical one.

It is also possible to have available values of both pressure (and thus area) and flux variations at the proximal section. For instance, measurements of

pressure pulse together with flux data could be obtained from Doppler ultrasound. Clearly the hyperbolic system does not allow to impose both conditions at the same time. However, one may construct a set of allowable boundary conditions through the exact or approximate solution of a Riemann problem [199] at the boundary using the computed values and the known values at the inlet. We will go back to this technique when we discuss the numerical treatment of the boundary data. Alternatively, one may set the incoming characteristics variables as

$$W_1(x_1, t) = W_1(\tilde{p}(t), \tilde{u}(t)),$$

where  $\tilde{p}(t)$  and  $\tilde{u}(t)$  are the given (measured) values of pressure and velocity, while  $W_1(p, u)$  denotes the analytic expression of  $W_1$  as function of these two variables. In both cases we are not enforcing pressure and velocity exactly (it is not compatible with the hyperbolic character of the differential problem).

### Distal boundary of terminal vessels: coupling with a model of peripheral circulation

The human arterial system is a network of large arteries branching out into many smaller arteries, arterioles and capillaries. We are usually interested in the results in the larger arteries in the network. Blood vessels further down the arterial tree are very small and numerous. They have, all together, an important role in determining the haemodynamics in the large arteries since they offer flow resistance and pressure wave is partially reflected at each bifurcation. An accurate description of all these vessels and districts although virtually possible is unfeasible for the huge amount of data required not to mention the computational costs. For these reasons, the downstream circulation is usually described in terms of lumped parameter models. In Section 10.2 we will introduce extensively these kind of models and their derivation. So, in general terms, an appropriate way for accounting outflow conditions is to resort to *multiscale models*, namely coupling 1D and lumped parameter models. Chapter 11 will be devoted to this topic. Here we limit ourselves to some considerations when the role of the lumped parameter models is only limited to provide a boundary condition for the 1D model, without further details on the peripheral circulation.

Denoting by  $\pi_T(\omega)$  and  $\chi_T(\omega)$  the Fourier transform of  $P_T(t) = P(x_{\text{out}}, t)$  and  $Q_T(t) = Q(x_{\text{out}}, t)$  respectively (see Chapter 2) at the end of the 1D network, the behaviour of the downstream network can be represented by the *terminal impedance* (see Fig. 10.14, left) as

$$\zeta_T(\omega) = \frac{\pi(\omega)}{\chi(\omega)}, \quad (10.43)$$

that in general is a complex-valued function. An extensive discussion about the role of the impedance function in describing the vascular tree haemodynamics can be found in Chapter 13 of [350]. Here the impedance is the *transfer function* describing in a simplified way the downstream blood dynamics

that actually influences the hemodynamics in the proximal district represented by our 1D model. The counterpart of (10.43) in the time domain is obtained by computing the inverse Fourier transform of the terminal impedance,  $Z_T = \mathcal{F}^{-1}(\zeta_T)$  and by applying the convolution theorem

$$p_T(t) = \int_{t-H}^t Z_T(t - \tau) Q_T(\tau) d\tau, \quad (10.44)$$

where  $H$  denotes the heart beat duration. Relation (10.44), possibly approximated with suitable numerical quadratures, provides the boundary condition to be used for the 1D network model in correspondence of terminal vessels.

Since possible examples of impedance functions used in the literature stem from the representation of the terminal districts by lumped parameter models, often represented in terms of electrical circuits, we postpone their description to the next section (see Section 10.2.3).

Relation (10.44) is not strictly of the form (10.41) and its admissibility for a general  $Z_T$  should be investigated. However, it has proved very effective in the several test cases carried out so far.

### 10.1.6 Numerical compatibility relations at the boundary

When calculating the numerical solution of our system we need to compute at the boundary points the values of both variables  $Q$  and  $A$  (or  $u$  and  $A$ ), yet the boundary condition provides only a single relation. We need to complete this piece of information with an additional relation that can only come from the differential equation. A possibility is to project the equation along the outgoing characteristics, giving rise to the so-called compatibility relations [408]. Again, for the sake of simplicity let us consider first the point  $x = x_1$  and the differential equation written in the quasi-linear form (10.35). The compatibility relation in this case reads

$$\mathbf{l}_2^T \left[ \frac{\partial \mathbf{U}}{\partial t} + \mathbf{H} \frac{\partial \mathbf{U}}{\partial x} - \mathbf{f}(\mathbf{U}) \right] = 0, \quad \text{at } x = x_1, \quad t > 0.$$

By simple manipulations it may be recognised that this expression may be written as

$$\frac{dW_2(x(t), t)}{dt} - \mathbf{l}_2^T \mathbf{f}(\mathbf{U}) = 0, \quad \text{at } x = x_1, \quad t > 0, \quad (10.45)$$

where  $\frac{dW_2(x(t), t)}{dt}$  is the total derivative of  $W_2$  along the characteristic curve of equation  $\frac{dx(t)}{dt} = \lambda_2$ .

In a numerical setting relation (10.45) may be approximated by following the characteristic line backwards. Using a first-order scheme we may set at  $t = t^{n+1} = t^n + \Delta t$  that

$$W_2(x_1, t^{n+1}) = W_2(x_1 - \lambda_2 \Delta t, t^n) + \Delta t \mathbf{l}_2^T \mathbf{f}(\mathbf{U}), \quad (10.46)$$

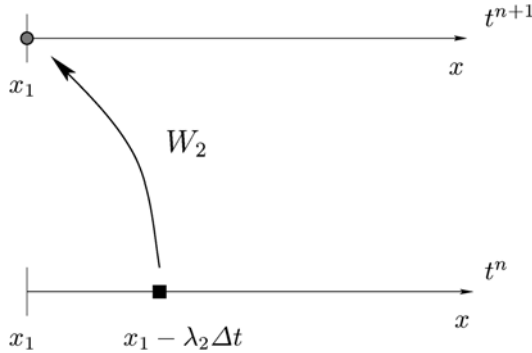


**Fig. 10.2.** Extrapolation of the characteristic  $W_2$  in  $x_1$

where  $\lambda_2$  and  $\mathbf{U}$  are computed at  $x = x_1$  and  $t = t^n$ . More accurate schemes may be devised following the ideas applied in [48] in the context of Navier-Stokes equations. Relation (10.46) is called *extrapolation of the characteristic variable*, and coupled with the boundary condition provides a full set of (non-linear) equations for the numerical computation of the boundary data. An analogous relation may be found at  $x = x_2$  for  $W_1$ .

We may note that if  $\mathbf{f} = \mathbf{0}$ , which is the case if we neglect the friction term, and the dependence of  $B$  and  $A_0$  on  $x$ , then (10.46) reduces to  $W_2(x_1, t^{n+1}) = W_2(x_1 - \lambda_2 \Delta t, t^n)$ .

### 10.1.7 Extensions of the basic model

In the previous sections we have introduced some assumptions on the geometry of the vessel and on the smoothness of the coefficients characterizing the wall dynamics. These hypotheses are acceptable for small segments of the vascular tree, however more general models should be introduced to deal with segments with discontinuous properties, bifurcations and curved vessels. These will be discussed in the following sections.

### Discontinuous material properties

In some cases, material properties of the wall are not smooth. In particular, coefficient  $\beta$  introduced in (10.21) features discontinuities for instance in stented arteries (Fig. 10.3) or in by-pass grafts. The Young’s modulus  $E$  can exhibit jumps due to the differences between the vascular tissue and the prosthesis (see e.g. [269]). It is also possible for the area of the vessel to change abruptly due to certain pathologies, e.g. an aneurysm.

Since the derivative of the elastic coefficient  $\beta$  appears in the balance of momentum equation, the presence of discontinuities in  $\beta$  requires careful treatment in our models. There are basically two approaches for handling material discontinuities.

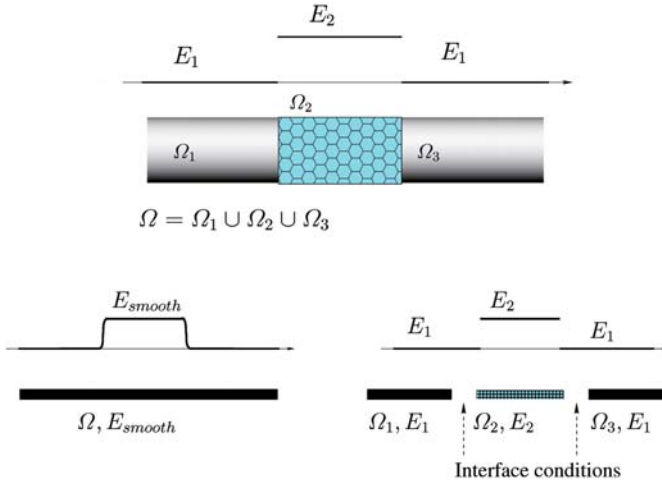


**Fig. 10.3.** Discontinuity of Young’s modulus in the case of a stented artery. Bottom left: regularisation approach; bottom right: domain splitting

1. *Data regularisation:* the discontinuous data are suitably replaced by smooth functions that can be differentiated and the models presented above can be used straightforwardly.
2. *Domain splitting:* the vessel with discontinuous properties is split into a set of smooth segments and the coupling between each pair of segments is accomplished through suitable *matching or interface conditions*. A reasonable choice is to assume continuity of fluxes and thus impose the continuity of mass flux and total pressure across the interface, i.e.

$$Q = u_l A_l = u_r A_r, \tag{10.47}$$

$$P_r = \rho \frac{u_l^2}{2} + \beta_l (\sqrt{A_l} - \sqrt{A_{l_0}}) = \rho \frac{u_r^2}{2} + \beta_r (\sqrt{A_r} - \sqrt{A_{r_0}}). \tag{10.48}$$

These interface conditions will preserve the conservation properties of the  $(A, u)$  system.

In practice, the problem can be solved iteratively, by solving the sequence of problems on each segment. In this case, the interface conditions (possibly reformulated in terms of characteristic variables) become boundary conditions on each segment, following a classical domain decomposition approach (see e.g. [408]).

### Treatment of bifurcations

The 1D model of the compliant tube can be extended to handle the arterial tree by adopting a domain splitting technique similar to the one used for the discontinuous case. Again we require suitable interface conditions at the bifurcations or branching points of the tree (see Fig. 10.4).

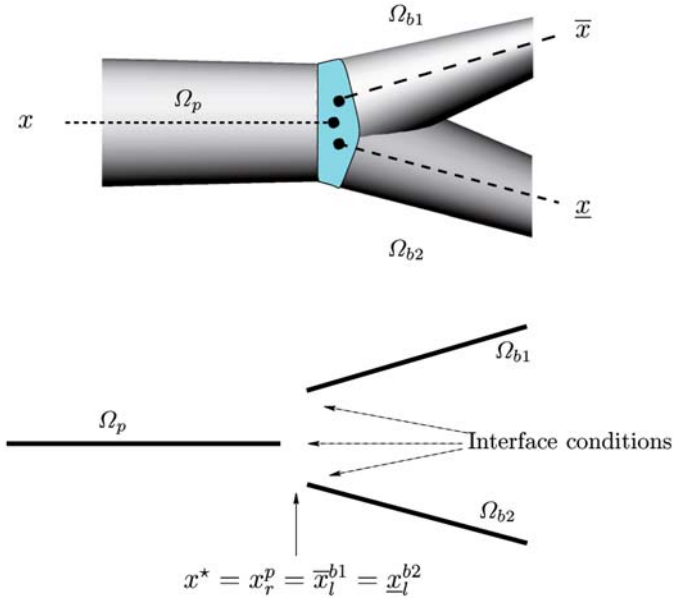


**Fig. 10.4.** Arterial tree bifurcation: notation

In the bifurcations the problem is only *locally* one-dimensional, in the sense that each branch is associated with its own axis (denoted by  $x$ ,  $\bar{x}$  and  $\underline{x}$  in Fig. 10.4). The use of domain splitting techniques allows us to cast the global problem into a set of 1D problems (10.27) or (10.28). If we denote by  $x^*$  the branching point such that it is the right-end point  $x_r^p$  of the parent vessel  $\Omega_p$ , and the left-end point  $\bar{x}_l^{b1}$  and  $\underline{x}_l^{b2}$  of the branches  $\Omega_{b1}$  and  $\Omega_{b2}$ , for a given function  $f$  defined over each segment we denote

$$f_l = f|_{\Omega_p}(x_r^p), \quad f_{b1} = f|_{\Omega_{b1}}(\bar{x}_l^{b1}), \quad f_{b2} = f|_{\Omega_{b2}}(\underline{x}_l^{b2}).$$

At the bifurcation we have six unknowns:  $(A_l, u_l)$  in the parent vessel,  $(A_{b1}, u_{b1})$  and  $(A_{b2}, u_{b2})$  in the branches  $\Omega_{b1}$  and  $\Omega_{b2}$  respectively.

The first three equations required to solve the problem may be obtained by extrapolating the outgoing characteristics like in (10.46) (or alternatively by solving (10.45)), giving

$$W_1 = u_l + 4A_l^{1/4} \sqrt{\frac{\beta_l}{2\rho}} = W_1^*, \tag{10.49}$$

$$W_{21} = u_{b1} - 4A_{b1}^{1/4} \sqrt{\frac{\beta_{b1}}{2\rho}}, \tag{10.50}$$

$$W_{22} = u_{b2} - 4A_{b2}^{1/4} \sqrt{\frac{\beta_{b2}}{2\rho}} = W_{22}^*, \tag{10.51}$$

where the starred quantities are the extrapolated values. The other three equations required to close the problem are obtained from the continuity of mass flux and total pressure across the boundary of the elements at the bifurcation, i.e.

$$Q = u_p A_p = u_{b1} A_{b1} + u_{b2} A_{b2}, \quad (10.52)$$

$$P_r = \rho \frac{u_p^2}{2} + \beta_p (\sqrt{A_p} - \sqrt{A_{p0}}) = \rho \frac{u_{b1}^2}{2} + \beta_{b1} (\sqrt{A_{b1}} - \sqrt{A_{b1_0}}), \quad (10.53)$$

$$P_r = \rho \frac{u_p^2}{2} + \beta_p (\sqrt{A_p} - \sqrt{A_{p0}}) = \rho \frac{u_{b2}^2}{2} + \beta_{b2} (\sqrt{A_{b2}} - \sqrt{A_{b2_0}}). \quad (10.54)$$

The six equations given by (10.49-10.54) define a non-linear system of algebraic equations which allow to determine the values of  $(A_l, u_l)$ ,  $(A_{r1}, u_{r1})$  and  $(A_{r2}, u_{r2})$  at the bifurcation. These values are then used to evaluate the flux at the elemental interfaces in the numerical discretisation.

We have assumed that the coefficient  $\beta$  could be different in the three vessels, as it is to be expected from the different values of their respective areas at rest  $A_0$ .

**Remark 10.1.3** *Continuity of the total pressure in (10.53,10.54) can be modified for including pressure losses due to the bifurcation. These typically depend on the bifurcation angle. For more details see [157, 469].*

### Accounting for curvature in 1D models (Directors' theory)

One of the most relevant assumptions in devising the basic 1D model is that the axis of the vessel is rectilinear. Actually, if we remove this hypothesis, it is still possible to define a main flow direction in the domain, namely the curvilinear abscissa along the axis, and however the effect of the blood dynamics in the other directions on the main one is no longer negligible (see [373]). Nevertheless, there are some vessels which are significantly curved (aorta, femoral arteries, etc.). For these vessels, the basic 1D model (10.28) or (10.27) can be considered only as a rough description. A possible model relies on introducing a subdivision into subsegments sufficiently short to be considered straight and connected one to the other with a suitable angle  $\theta \neq 0$  (see Fig. 10.5). A suitable pressure loss as a function of the angle needs to be introduced in the interface conditions between segments. The other interface conditions will be given by the flow conservation (see (10.47) and Remark 10.1.3).

We would like to briefly address in the following an alternative definition of 1D models that are able to account for the effects of the transversal dynamics on the axial one, still at a reasonable computational cost. The task is not easy, since we want to devise a sort of 1D models for the cheap description of a genuinely 3D dynamics.

Simplified models for curved pipes can be obtained for small curvatures of the vessels with a perturbation analysis of the rectilinear model (see [113]).

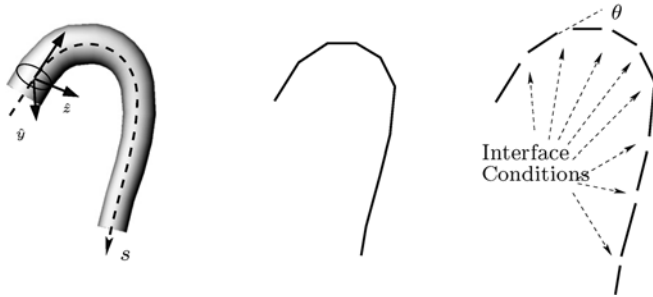


**Fig. 10.5.** Splitting of a curved domain into a sequence of rectilinear segments

Let us consider the non-dimensional parameter

$$De = 2\sqrt{2}\sqrt{\frac{r_w}{r_c}}\text{Re}, \tag{10.55}$$

where  $r_w$  is the vessel radius,  $r_c$  is the curvature radius of the vessel axis ( $r_c \rightarrow \infty$  in the straight case),  $\text{Re}$  is the *Reynolds number* and  $De$  the *Dean number* (they have been defined in Chapter 5). Simplified models can be readily obtained for small values of the Dean number. For large values of  $De$  these models need to be suitably corrected, and the analysis becomes by far more difficult: a complete description of this approach can be found in [373], Chapter 4.

A different approach relies on the *theory of Cosserat curves* considered by Green and Naghdi in [204,205] (see also [269]). If we consider the reference frame  $(s, \hat{y}, \hat{z})$  of Fig. 10.5 left, the basic idea of the Green and Naghdi approach is to represent the velocity field  $\mathbf{u}(s, \hat{y}, \hat{z}, t)$  with respect to a set of *shape functions* that depend only on the coordinates in the normal section  $\hat{y}, \hat{z}$  and are given by

$$\mathbf{u}(s, \hat{y}, \hat{z}, t) = \sum_{n=0}^N \omega_n(s, t)\boldsymbol{\varphi}(\hat{y}, \hat{z}), \tag{10.56}$$

where  $\omega_n$  are the coefficients of the velocity profile. This can be considered as a generalisation of the straight vessel case, where we set for the axial velocity,  $u_z(x, y, z, t) = \varphi(\hat{y}, \hat{z})\bar{u}(x, t)$  being  $\bar{u}(x, t)$  the average velocity and  $\varphi(\hat{y}, \hat{z})$  a given velocity profile. Once a basis function set is selected the unknowns are the coefficients  $\omega_n$ , that can be computed by solving a suitable set of equations derived by mass and momentum conservation principles.

In principle, the accuracy of these models can be tuned by choosing a suitably large  $N$ , i.e. having a rich enough basis functions set. However, even for small values of  $N$ , mathematical difficulties of the obtained model imply high numerical costs (see [269]).

### A curved pipe model

Let us consider a curved pipe of circular section and indicate by  $s$  the arch length coordinate of the axis, which we assume to be a planar curve. If we integrate any function  $f(s, \hat{y}, \hat{z}, t)$  over the volume of the pipe  $V(\varepsilon)$  between normal sections at a distance  $\varepsilon$  one to the other and let  $\varepsilon \rightarrow 0$ , we get (see [269])

$$\lim_{\varepsilon \rightarrow 0} \frac{1}{\varepsilon} \int_{\bar{s}-\varepsilon/2\mathcal{S}}^{\bar{s}+\varepsilon/2} \int \sqrt{g} f(\bar{s}, \hat{y}, \hat{z}, t) d\sigma ds = \int_{\mathcal{S}} \sqrt{g} f(\bar{s}, \hat{y}, \hat{z}, t) d\sigma,$$

where  $\mathcal{S} = \mathcal{S}(\bar{s}, t)$  is the section normal to the vessel axis and  $\sqrt{g}$  is the metric tensor invariant, accounting for the integration over a curved axis. In particular, for a rectilinear pipe  $g = 1$ , while for a curved vessel in the plane  $(s, y)$  with a constant curvature radius  $R_C$ ,  $\sqrt{g} = (\hat{y} + R_C)/\hat{y}$ .

Associated to this integral over the section  $\mathcal{S}$ , we introduce the following operators acting on a generic regular enough function  $f(\bar{s}, \hat{y}, \hat{z}, t)$

$$\begin{aligned} P_{00}(f) &= \int_{\mathcal{S}} \sqrt{g} f d\hat{y} d\hat{z}, \\ P_{10}(f) &= \int_{\mathcal{S}} \sqrt{g} f \hat{y} d\hat{y} d\hat{z}, \quad P_{01}(f) = \int_{\mathcal{S}} \sqrt{g} f \hat{z} d\hat{y} d\hat{z}. \end{aligned} \tag{10.57}$$

Consider now the 3D Navier-Stokes equations written with respect to the reference frame  $(s, \hat{y}, \hat{z})$  with the velocity field represented by (10.56). In particular, we assume for the axial velocity

$$u_s = \left( 1 - \frac{\hat{y}^2 + \hat{z}^2}{R^2} \right) (a(s, t) + b(s, t)\hat{y} + c(s, t)\hat{z}),$$

which is a generalisation of the classical parabolic profile (first term), while for the transversal velocity components, we simply postulate a linear dependence:  $u_{\hat{y}} = \hat{\eta}\hat{y}/R$ ,  $u_{\hat{z}} = \hat{\eta}\hat{z}/R$ , where  $\hat{\eta}$  is the wall velocity. The unknowns of the problem are therefore the coefficients  $a(s, t)$ ,  $b(s, t)$  and  $c(s, t)$  and the vessel radius  $R(s, t)$ . A more convenient set of unknowns is

$$A = \pi R^2, \quad Q = \frac{\pi}{2} R^2 a, \quad H = \frac{\pi}{12} R^4 b, \quad G = \frac{\pi}{12} R^4 c.$$

For the determination of these unknowns we need four equations that can be obtained by applying memberwise the average operator  $P_{00}$  to the continuity equation and the operators  $P_{00}$ ,  $P_{10}$  and  $P_{01}$  to the axial momentum equations.

The resulting 1D model for curved vessels reads

$$\left\{ \begin{array}{l} \frac{\partial A}{\partial t} + \frac{\partial Q}{\partial s} = 0, \\ \frac{\partial Q}{\partial t} + \frac{4}{3} \frac{\partial}{\partial s} \left( \frac{Q^2}{A} \right) + 6\pi \frac{\partial}{\partial s} \left( \frac{H^2}{A^2} \right) + \\ \qquad 6\pi \frac{\partial}{\partial s} \left( \frac{G^2}{A^2} \right) + \frac{\beta\sqrt{A}}{2\rho A_0} \frac{\partial A}{\partial s} + 8\pi\nu \frac{Q}{A} = 0, \\ \frac{\partial H}{\partial t} + \frac{H}{2A} \frac{\partial Q}{\partial s} + 2 \frac{\partial}{\partial s} \left( \frac{HQ}{A} \right) + 24\pi\nu \frac{H}{A} = 0, \\ \frac{\partial G}{\partial t} + \frac{G}{2A} \frac{\partial Q}{\partial s} + 2 \frac{\partial}{\partial s} \left( \frac{GQ}{A} \right) + 24\pi\nu \frac{G}{A} = 0. \end{array} \right. \quad (10.58)$$

More complex model can be devised for instance by assuming a different profile for the transversal velocity components (see [269]).

### 10.1.8 The numerical solution of the 1D models

The wave propagation speeds in the large arteries are typically an order of magnitude higher than the average flow speeds. As mentioned previously, the characteristic system is inherently subcritical and does not produce shock under physiological conditions. Therefore the numerical challenge is to propagate waves for many periods without suffering from excessive errors in amplitude (*dissipation*) and in phase (*dispersion*) (see e.g. [277]). If the solution remains smooth then high-order methods are particularly attractive due to the fast convergence of the dispersion and dissipation errors with the order of the scheme [457].

Here, we limit ourselves to present two possible discretisations of the problems. The first one is based on a *Taylor-Galerkin approach* and is essentially a generalisation of the classical *Lax-Wendroff* scheme for systems of conservation laws (see [277]).

The second one is based on more recent techniques for the discretisation of the space variable, in which continuity of the solution at the discretisation nodes is no longer postulated. This *discontinuous Galerkin approach* is well suited for high order approximations.

#### Taylor-Galerkin method

In this section we describe the numerical discretisation of the  $(Q, A)$  system described by equation (10.27) recast in the conservation form (10.31) given by

$$\frac{\partial \mathbf{Q}}{\partial t} + \frac{\partial \mathbf{G}}{\partial x}(\mathbf{Q}) = \mathbf{B}(\mathbf{Q}).$$

The expressions for  $\mathbf{Q}$ ,  $\mathbf{G}$  and  $\mathbf{B}$  are given in (10.30).

We proceed to discretise equation (10.31) by adopting a second-order Taylor-Galerkin scheme. To this aim, we write the Taylor expansion truncated up to the second order terms at time  $t^n$  such that  $\Delta t = t^{n+1} - t^n$ , yielding

$$Q^{n+1} = Q^n + \Delta t \left. \frac{\partial Q}{\partial t} \right|^n + \frac{\Delta t^2}{2} \left. \frac{\partial^2 Q}{\partial t^2} \right|^n. \tag{10.59}$$

The time derivatives will be replaced by space derivatives, by exploiting the equations (10.31). In particular, we will use the abridged notation

$$G_Q = \frac{\partial G}{\partial Q}, \quad B_Q = \frac{\partial B}{\partial Q},$$

and we obtain

$$\frac{\partial Q}{\partial t} = B - \frac{\partial G}{\partial x}, \tag{10.60}$$

$$\begin{aligned} \frac{\partial^2 Q}{\partial t^2} &= B_Q \frac{\partial Q}{\partial t} - \frac{\partial^2 G}{\partial t \partial x} = B_Q \frac{\partial Q}{\partial t} - \frac{\partial}{\partial x} \left( G_Q \frac{\partial Q}{\partial t} \right) = \\ &B_Q \left( B - \frac{\partial G}{\partial x} \right) - \frac{\partial (G_Q B)}{\partial x} + \frac{\partial}{\partial x} \left( G_Q \frac{\partial G}{\partial x} \right). \end{aligned} \tag{10.61}$$

**Remark 10.1.4** *The presence of a non-constant source term and the explicit dependence of the momentum flux  $G$  on the variable  $x$  through  $\beta(x)$  makes the derivation of the scheme slightly more complex than the standard Lax-Wendroff formulation. In particular we stress that, in contrast to the normal derivation, we have not further developed the  $x$  derivative of the fluxes, since for our problem*

$$\frac{\partial G}{\partial x} \neq G_Q \frac{\partial Q}{\partial x},$$

because of the dependence of  $G$  on  $x$  through  $\beta$ .

From (10.59), (10.60) and (10.61) we obtain the following time-marching scheme

$$\begin{aligned} Q^{n+1} &= Q^n - \Delta t \frac{\partial}{\partial x} \left[ G^n + \frac{\Delta t}{2} G_Q^n B^n \right] - \frac{\Delta t^2}{2} \left[ B_Q^n \frac{\partial G^n}{\partial x} \right. \\ &\quad \left. - \frac{\partial}{\partial x} \left( G_Q^n \frac{\partial G^n}{\partial x} \right) \right] + \Delta t \left( B^n + \frac{\Delta t}{2} B_Q^n B^n \right). \end{aligned} \tag{10.62}$$

Space discretisation is carried out by using linear finite elements. To that purpose, let us subdivide the domain  $\Omega$  into  $N_{el}$  finite elements  $\Omega_e$ , of size  $h_e$ . We indicate by  $\mathbf{V}_h$  the space of continuous vector functions defined on  $\Omega$ , linear on each element, and with  $\mathbf{V}_h^0$  the set formed by functions of  $\mathbf{V}_h$  which are zero at  $x = x_1$  and  $x = x_2$ . Furthermore, we omit the subscript  $\Omega$  in the  $\mathbf{L}^2(\Omega)$  vector product.

Using the notation

$$\begin{aligned} \mathbf{G}_{LW} &= \mathbf{G} + (\Delta t/2)\mathbf{G}_Q\mathbf{B}, \\ \mathbf{B}_{LW} &= \mathbf{B} + (\Delta t/2)\mathbf{B}_Q\mathbf{B}, \end{aligned}$$

and indicating with

$$(\mathbf{u}, \mathbf{v})_\Omega = \int_\Omega \mathbf{u} \mathbf{v} \, dx,$$

the standard  $\mathbf{L}^2(\Omega)$  inner product, the finite element solution of (10.62) requires, for  $n \geq 0$ , to find  $\mathbf{Q}_h^{n+1}$  in  $\mathbf{V}_h$  which satisfies for all  $\psi_h$  in  $\mathbf{V}_h^0$  that

$$\begin{aligned} (\mathbf{Q}_h^{n+1}, \psi_h) &= (\mathbf{Q}_h^n, \psi_h) + \Delta t(\mathbf{G}_{LW}^n, \frac{\partial \psi_h}{\partial x}) - \frac{\Delta t^2}{2}(\mathbf{B}_Q^n \frac{\partial \mathbf{G}^n}{\partial x}, \psi_h) - \\ &\frac{\Delta t^2}{2}(\mathbf{G}_Q^n \frac{\partial \mathbf{G}^n}{\partial x}, \frac{\partial \psi_h}{\partial x}) + \Delta t(\mathbf{B}_{LW}^n, \psi_h). \end{aligned} \tag{10.63}$$

The numerical initial condition  $\mathbf{U}_h^0$  will be taken as the finite element interpolant of the given initial data  $\mathbf{U}_0$ . A possible technique for computing the boundary values  $\mathbf{U}_h^{n+1}$  is described later on.

In (10.63) we need to numerically integrate the terms containing the fluxes and sources. For the terms involving  $\mathbf{G}^n$  and  $\mathbf{G}_Q^n$  we have projected each component on the finite element function space  $V_h$  via interpolation. The same applies for the other vector products which involve only  $\mathbf{G}^n$  and  $\mathbf{G}_Q^n$ .

The term  $d\beta/dx$  in  $\mathbf{B}^n$  and  $\mathbf{B}_Q^n$  must be approximated in a piecewise constant manner to ensure that our numerical scheme represents constant solutions of the differential problem exactly. Therefore, on each element  $(x_e^l, x_e^u)$  we have approximated  $d\beta/dx$  by  $[\beta(x_i^u) - \beta(x_i^l)]/h_e$ . For the remaining terms we have applied the same technique adopted for the fluxes. This gives rise to a piecewise linear discontinuous representation for the source terms.

### Discontinuous Galerkin method

The discontinuous Galerkin method is an attractive formulation for high-order discretisation of hyperbolic conservation laws. Following the work of Cockburn and Shu [96] and Lomtev, Quillen and Karniadakis [296] we proceed as follows.

Considering the one-dimensional hyperbolic system (10.28) in conservative form we have

$$\frac{\partial \mathbf{U}}{\partial t} + \frac{\partial \mathbf{F}}{\partial x} = \mathbf{S}(\mathbf{U}), \tag{10.64}$$

where

$$\mathbf{U} = \begin{bmatrix} U_1 \\ U_2 \end{bmatrix} = \begin{bmatrix} A \\ u \end{bmatrix}, \quad \mathbf{F} = \begin{bmatrix} F_1 \\ F_2 \end{bmatrix} = \begin{bmatrix} uA \\ \frac{u^2}{2} + \frac{p}{\rho} \end{bmatrix}, \quad \mathbf{S} = \begin{bmatrix} S_1 \\ S_2 \end{bmatrix} = \begin{bmatrix} 0 \\ -K_R \frac{u}{A} \end{bmatrix}.$$

To solve this system in a domain  $\Omega = (x_1, x_2)$  discretised into a mesh of  $N_{el}$  elemental non-overlapping regions  $\Omega_e = (x_e^l, x_e^u)$ , such that  $x_e^u = x_{e+1}^l$  for  $e = 1, \dots, N_{el}$ , and

$$\bigcup_{e=1}^{N_{el}} \overline{\Omega}_e = \overline{\Omega},$$

we start by constructing the weak form of (10.64), i.e.

$$\left( \frac{\partial \mathbf{U}}{\partial t}, \boldsymbol{\psi} \right)_{\Omega} + \left( \frac{\partial \mathbf{F}}{\partial x}, \boldsymbol{\psi} \right)_{\Omega} = (\mathbf{S}, \boldsymbol{\psi})_{\Omega}, \quad (10.65)$$

where  $\boldsymbol{\psi}$  represents an arbitrary function in  $\Omega$ . Decomposing the integral into elemental regions we obtain

$$\sum_{e=1}^{N_{el}} \left[ \left( \frac{\partial \mathbf{U}}{\partial t}, \boldsymbol{\psi} \right)_{\Omega_e} + \left( \frac{\partial \mathbf{F}}{\partial x}, \boldsymbol{\psi} \right)_{\Omega_e} - (\mathbf{S}, \boldsymbol{\psi})_{\Omega_e} \right] = 0. \quad (10.66)$$

Integrating the second term by parts leads to

$$\sum_{e=1}^{N_{el}} \left[ \left( \frac{\partial \mathbf{U}}{\partial t}, \boldsymbol{\psi} \right)_{\Omega_e} - \left( \mathbf{F}, \frac{d\boldsymbol{\psi}}{dx} \right)_{\Omega_e} + [\boldsymbol{\psi} \cdot \mathbf{F}]_{x_e^u} - (\mathbf{S}, \boldsymbol{\psi})_{\Omega_e} \right] = 0. \quad (10.67)$$

To get the discrete form of our problem we choose  $\mathbf{U}$  to be in the finite space of  $\mathbf{L}^2(\Omega)$  functions which are polynomial of degree  $q$  on each element. We indicate an element of such space using the subscript  $h$ . We also note that  $\mathbf{U}_h$  may be discontinuous across inter-element boundaries. However to attain a global solution in the domain  $\Omega$  we need to allow information to propagate between the elemental regions. Information is propagated between elements by upwinding the boundary flux,  $\mathbf{F}$ , in the third term of equation (10.67).

More precisely, thanks to the relations (10.39) linking primitive and characteristic variables we may always write the flux  $\mathbf{F}$  as function of the characteristic variables, that is  $\mathbf{F} = \mathbf{F}(W_1, W_2)$ . At the right interface of element  $\Omega_e$  we set the upwinded flux as  $\mathbf{F}^u = \mathbf{F}(W_1^-, W_2^+)$ , being  $W_1^+ = W^1|_{\Omega_e(x_e^l)}$  and  $W_2^- = W^2|_{\Omega_{e+1}(x_{e+1}^r)}$ , being  $\Omega_{e+1}$  the adjacent element on the right of  $\Omega_e$ . On the left interface the relation is analogous with the role of  $W_1$  and  $W_2$  exchanged. In this way we always construct the flux by using the information carried by the two characteristics impinging on the interface. This upwinding process can be conveniently used in the numerical scheme also to impose the boundary conditions, as we will see in the next section. Clearly we are assuming that the flow is subcritical, i.e.  $\lambda_1 > 0$  and  $\lambda_2 < 0$ .

The discrete weak formulation can now be written as

$$\sum_{e=1}^{N_{el}} \left\{ \left( \frac{\partial \mathbf{U}_h}{\partial t}, \boldsymbol{\psi}_h \right)_{\Omega_e} - \left( \mathbf{F}(\mathbf{U}_h), \frac{d\boldsymbol{\psi}_h}{dx} \right)_{\Omega_e} + [\boldsymbol{\psi}_h \cdot \mathbf{F}^u]_{x_e^u} - (\mathbf{S}(\mathbf{U}_h), \boldsymbol{\psi}_h)_{\Omega_e} \right\} = 0. \quad (10.68)$$

Following the traditional Galerkin approach, we choose the test function  $\psi_h$  within each element to be in the same discrete space as the numerical solution  $\mathbf{U}_h$ . At this point if we defined our polynomial basis and choose an appropriate quadrature rule we would now have a semi-discrete scheme. However, from an implementation point of view, the calculation of the second term in equation (10.68) can be inconvenient and consequently we choose to integrate this term by parts once more to obtain

$$\sum_{e=1}^{N_{el}} \left\{ \left( \frac{\partial \mathbf{U}_h}{\partial t}, \psi_h \right)_{\Omega_e} + \left( \frac{\partial \mathbf{F}(\mathbf{U}_h)}{\partial x}, \psi_h \right)_{\Omega_e} + [\psi_h \cdot \{\mathbf{F}^u - \mathbf{F}(\mathbf{U}_h)\}]_{x_e^l}^{x_e^u} - (\mathbf{S}(\mathbf{U}_h), \psi_h)_{\Omega_e} \right\} = 0. \tag{10.69}$$

We note that the information between elements is transmitted by the third boundary term as the difference between the upwinded and the local fluxes,  $[\psi_h \cdot \{\mathbf{F}^u - \mathbf{F}(\mathbf{U}_h)\}]_{x_e^l}^{x_e^u}$ . This method can be considered as a penalty method with an automatic procedure for determining the penalty parameter.

Finally we select our expansion bases to be polynomials of order  $q$  and expand our solution on each element  $e$  in terms of Legendre polynomials  $L_p(\xi)$ , i.e.

$$\mathbf{U}_h|_{\Omega_e}(x_e(\xi), t) = \sum_{p=0}^q L_p(\xi) \hat{\mathbf{U}}_e^p(t).$$

where, following standard finite element techniques, we consider  $\xi$  in the reference element  $\Omega_{\text{ref}} = \{\xi : -1 \leq \xi \leq 1\}$  and introduce the elemental affine mapping

$$x_e(\xi) = x_e^l \frac{(1 - \xi)}{2} + x_e^u \frac{(1 + \xi)}{2}$$

whose Jacobian  $J_e$  is

$$J_e = \frac{dx_e}{d\xi} = \frac{x_e^u - x_e^l}{2}.$$

We note that the choice of discontinuous discrete solution and test functions allows us to decouple the problem on each element, the only link coming through the upwinded boundary fluxes. Legendre polynomials are particularly convenient because the basis is orthogonal with respect to the  $\mathbf{L}^2(\Omega_e)$  inner product and equation (10.69) turns out to be equivalent to solving component-wise, for all elements  $e$ , for  $i = 1, 2$  and  $p = 1, \dots, P$ , the equation

$$J_e \frac{\partial \hat{U}_{i,e}^p}{\partial t} = -J_e \left( \frac{\partial F_i}{\partial x}, L_p \right)_{\Omega_e} - [L_p (F_i^u - F_i(\mathbf{U}_h))]_{x_e^l}^{x_e^u} + J_e (S_i, L_p)_{\Omega_e}. \tag{10.70}$$

To complete the discretisation we require a time integration scheme. Possible choices are the standard Runge-Kutta or the Adams-Bashforth schemes (see e.g. [403]).

## The numerical treatment of boundary data

The numerical schemes (10.70) and (10.63) need to be complemented with boundary data  $\mathbf{Q}$  or  $\mathbf{U}$  at the boundaries of the domain  $\Omega$ . The way the boundary data is treated in practice by the two schemes is different.

### *Taylor-Galerkin method*

Let assume that the boundary condition at  $x = x_1$  is given by the general form (10.41). A possible way to provide the boundary data on the first node at time  $t^{n+1}$ , here indicated by  $\mathbf{Q}_0^{n+1}$  is to solve the system

$$\begin{aligned} \varphi(\mathbf{Q}_0^{n+1}) &= g(t^{n+1}), \\ W_2(\mathbf{Q}_0^{n+1}) &= W_2^* = W_2(x_1 - \lambda_2 \Delta t, t^n) + \Delta t \mathbf{I}_2^T \mathbf{f}, \end{aligned} \quad (10.71)$$

where  $\lambda_2$  and  $\mathbf{f}$  are computed, for instance, in  $x = x_1$  and at  $t = t^n$  and  $W_2(\mathbf{Q})$  indicates the expression linking the characteristic and primitive variables that can be derived from (10.38).

It is a system of nonlinear equation which may be solved by a few Newton iterations, starting from the values at the previous time step. In practice, we have notices that for our problems three Newton iterations are sufficient.

Similar considerations can be applied to the right boundary  $x_2$ .

### *Discontinuous Galerkin method: Flux upwinding*

The procedure illustrated in the previous paragraph may in principle be applied also to the discontinuous Galerkin scheme. However in the latter the technique of flux upwinding at the interface between elements may be of hand also to implement the boundary conditions. Let consider the boundary  $x = x_1$  and assume to have at disposal the boundary condition in terms of the entering characteristic, variable, i.e  $W_1 = w_1(t)$ . Then when computing the upwinded flux for the left interface of the first element we will set  $\mathbf{F}^u = \mathbf{F}(w(t^n), W_2^+)$ . If both primitive variables are provided at the boundary (for instance form experiments)  $w_1(t^n)$  could be readily computed from their value. It means that we will not impose the values exactly (it would be impossible because we can impose only a single scalar equation) but their value mediated through the entering characteristic variable. If instead we wish to impose the value of a single primitive variable, for instance the flux, the situation is more complicated.

## 10.2 Zero-dimensional (0D) or lumped models

As for the 1D models, lumped parameters models can be derived by general conservation principles or directly by averaging 3D and 1D models. In the former case, the key concept is the *compartment*, that is a part of the system at

hand that it is worth to be considered as a homogeneous unit. This definition is kept vague since the number and kind of compartments considered depend on the type of analysis at hand. A few compartments, describing the heart, arterial and venous systems and the capillary bed are sufficient for a very general description of the behaviour of the cardiovascular system. More detailed analysis may give rise to models with up to fifty separate compartments accounted for. Following this approach the continuous space dependence is lost, and the emphasis is on the behaviour of the unit with respect to the rest of the system. Input/output relations are formulated via transfer functions based either on physical or empirical relations.

Since we have already considered one-dimensional models of a blood vessel, we will here derive the corresponding lumped model by an averaging procedure. This approach is closer to the physics of the problem, and is useful to understand the role of the parameters of the model and their quantification. We will start from lumped parameter models of a simple vascular compartment formed by a single artery, and then, by application of appropriate matching conditions derived from conservation principles we will be able to build more general models.

Let us consider the single artery  $\Omega$ , illustrated in Fig. 10.1, of length  $l = |x_2 - x_1|$ . We define the (volumetric) mean flow rate over the whole artery as the quantity

$$\hat{Q} = \frac{\rho}{l} \int_{\Omega} u_1 dv = \frac{\rho}{l} \int_{x_1}^{x_2} \left( \int_{\mathcal{S}(x)} u_x d\sigma \right) dx = \frac{\rho}{l} \int_{x_1}^{x_2} Q(x) dx. \quad (10.72)$$

Similarly, we define the mean pressure and area over the artery as

$$\hat{p} = \frac{1}{l} \int_{x_1}^{x_2} P dx, \quad \hat{A} = \frac{1}{l} \int_{x_1}^{x_2} A dx. \quad (10.73)$$

Starting from equations (10.27) for this domain, we integrate the continuity equation along the axial direction ( $x_1 \leq x \leq x_2$ ) to obtain

$$l \frac{d\hat{A}}{dt} + Q_2 - Q_1 = 0, \quad (10.74)$$

where we have set

$$Q_1(t) = Q(t, x_1), \quad Q_2(t) = Q(t, x_2). \quad (10.75)$$

Observe that now  $\hat{A}$  depends only on time, so we have an ordinary time derivative.

In considering the momentum equation, we add the following simplifying assumptions:

1. *the contribution of the convective term  $\partial_x(\alpha Q^2/A)$  may be neglected; and*
2. *the variation of  $A$  (and  $\beta$ ) with respect to  $x$  is small compared to that of  $P$  and  $Q$ .*

The first assumption is particularly suited to represent the peripheral circulation, where blood flow is in general quite slow. The second assumption is reasonable when the axial average is carried out over short segments. It basically amounts to replace  $A$  in the momentum equation with a constant value for the area that in general is assumed to be the area at rest  $A_0$ . With these assumptions, averaging over  $x$  of (10.27)<sub>2</sub> yields

$$\frac{\rho l}{A_0} \frac{d\hat{Q}}{dt} + \frac{\rho K_R l}{A_0^2} \hat{Q} + P_2 - P_1 = 0, \quad (10.76)$$

where

$$P_1(t) = P(t, x_1), \quad P_2(t) = P(t, x_2). \quad (10.77)$$

As for 1D models we have now the problem of closing system (10.74, 10.76), by adding a wall mechanics law. In particular, if we assume the simple law (10.21) to hold, we have

$$\int_{x_1}^{x_2} \frac{\partial p}{\partial t} dx = \int_{x_1}^{x_2} \frac{\beta}{2\sqrt{A}} \frac{\partial A}{\partial t} dx.$$

Now, if we exploit the second assumption above, we obtain  $l \frac{d\hat{p}}{dt} = \frac{l\beta}{2\sqrt{A_0}} \frac{d\hat{A}}{dt}$ , which we write, for convenience, as

$$\frac{d\hat{A}}{dt} = k_1 \frac{d\hat{p}}{dt}, \quad (10.78)$$

where  $k_1 = \frac{\sqrt{A_0}}{\beta}$ . Substituting (10.78) into (10.74) we obtain

$$k_1 l \frac{d\hat{p}}{dt} + Q_2 - Q_1 = 0, \quad (10.79)$$

that together with (10.76) represents the lumped parameter model for a vessel.

Equations of this type are also found in the analysis of electrical circuits. Indeed, before digital computers, early simulations of flow in the vascular system were based on analog electrical circuits, see for instance [539]. In the electric network analogy, the blood flow rate is assimilated to the current, while blood pressure corresponds to voltage, as summarised in Table 10.1.

**Table 10.1.** Correspondence table of the analogy between electric and hydraulic networks

<i>Hydraulic</i>	<i>Electric</i>
<i>Pressure</i>	<i>Voltage</i>
<i>Flow rate</i>	<i>Current</i>
Blood viscosity	Resistance $R$
Blood inertia	Inductance $L$
Wall compliance	Capacitance $C$

In order to exploit this electrical analogy, we recast the system (10.76,10.79) as

$$\begin{aligned}
 C \frac{d\hat{p}}{dt} + Q_2 - Q_1 &= 0, \\
 L \frac{d\hat{Q}}{dt} + R\hat{Q} + P_2 - P_1 &= 0.
 \end{aligned}
 \tag{10.80}$$

The coefficients  $R$ ,  $L$  and  $C$  are associated to elements of a circuit as depicted in Fig. 10.6, where the corresponding equation is recalled at the bottom. We recall hereafter their physical significance.

**Resistance.** The coefficient  $R = \frac{\rho K_R l}{A_0^2}$  in equation (10.80) represents the *resistance* induced to the flow by the blood viscosity. Different expressions for  $R$  can be obviously obtained for different velocity profiles or if a non-Newtonian rheology is introduced into the model (see e.g. [426], [539], [162]).

**Inertia (inductance).** The coefficient  $L = \frac{\rho l}{A_0}$  in equation (10.76) represents the inertial term in the momentum equation and it will be called the *inductance* of the flow.

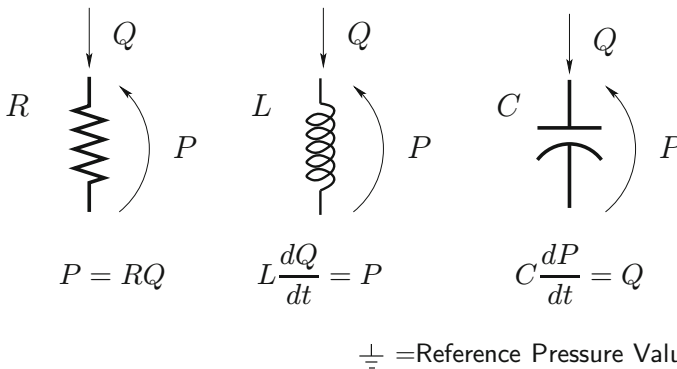


**Fig. 10.6.** Notation used in the electrical analogy of the circulatory system

**Compliance (capacitance).** It is characterised by the coefficient  $C = k_1 l$  that represents the mass storage term in the mass conservation law, due to the *compliance* of the vessel.

For instance, if we assume Poiseuille flow (i.e. fully developed flow with a constant pressure gradient) and that the vessel is a cylinder of constant circular section we have

$$R = \frac{8\pi\rho\nu l}{\pi^2 r_0^4} = \frac{8\mu l}{\pi r_0^4}; \quad L = \frac{\rho l}{\pi r_0^2}; \quad C = \frac{3\pi r_0^3 l}{2Eh_0}.$$

The system of equations (10.80) involves the mean flow rate and pressure over the vascular segment at hand and the *boundary* values of pressure and flow rate  $Q_i, P_i$ , with  $i = 1, 2$ . Strictly speaking, the term *boundary* is inappropriate, since the continuous space dependence has been lost in the axial average, and they simply represent input/output quantities exchanged by the vessel with the rest of the systems. However, we will retain the term, since it is related to the physical derivation of the equations. In particular, in order to close problem (10.80), we need to introduce some *boundary conditions*. This means that we need to identify the *input data* of the district at hand. For instance, suppose that  $Q_1$  and  $P_2$  are given. Then, (10.80) represents a system of two equations for four unknowns,  $\hat{Q}, \hat{p}, P_1$  and  $Q_2$ . The dynamic of the system is represented by  $\hat{p}$  and  $\hat{Q}$ , i.e. by the unknowns that are under time derivative (the *state variables*). We approximate now the unknowns on the upstream and downstream sections with the state variables,

$$\hat{p} \approx P_1, \quad \hat{Q} \approx Q_2,$$

that corresponds to assume that the *output* of the district is given by the *state variables*. With these additional assumptions, which are reasonable for a short pipe, the lumped parameter model becomes:

$$\begin{aligned} C \frac{dP_1}{dt} + Q_2 &= Q_1, \\ L \frac{dQ_2}{dt} + RQ_2 - P_1 &= P_2. \end{aligned} \tag{10.81}$$

where the input data have been put on the right hand side. This system can be illustrated by the electric  $\mathcal{L}$ -network shown in Fig. 10.7 (left).

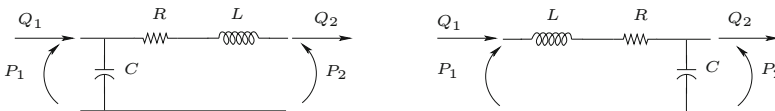


**Fig. 10.7.** Lumped  $\mathcal{L}$ -network (top) and  $\mathcal{L}$ -inverted network (bottom) equivalent to a short pipe

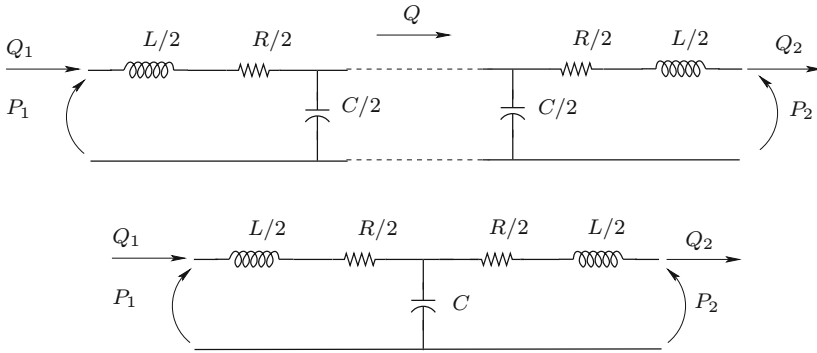


**Fig. 10.8.** Cascade connection of a  $\mathcal{L}$ -inverted and a  $\mathcal{L}$ -network (top), lumped  $\mathcal{T}$ -network (bottom)

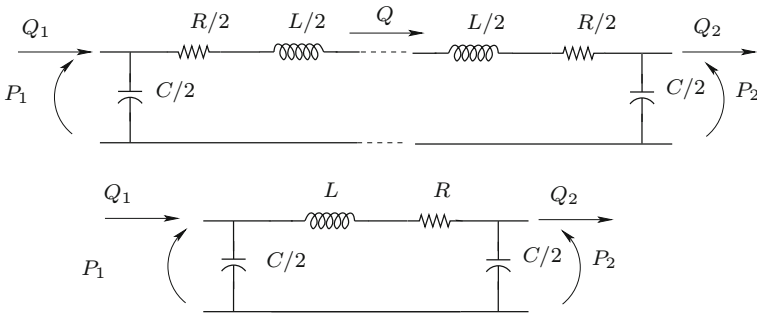


**Fig. 10.9.** Cascade connection of a  $\mathcal{L}$ -network and a  $\mathcal{L}$ -inverted one (top), lumped  $\pi$ -network (bottom)

In a similar way, if the pressure  $P_1$  and the flow rate  $Q_2$  are prescribed, we still approximate the quantities at the upstream and downstream sections by the state variables, i.e.  $\hat{p} \approx P_2$ ,  $\hat{Q} \approx Q_1$ , yielding the system represented by an electric analog, called an  $\mathcal{L}$ -inverted network, depicted in Fig. 10.7(right).

If the mean pressures  $P_1$  and  $P_2$  are prescribed, the system can be modelled by a cascade connection of  $\mathcal{L}$  and  $\mathcal{L}$ -inverted lumped representations, yielding a  $\mathcal{T}$ -network (Fig. 10.8). Similarly, if both flow rates  $Q_1$  and  $Q_2$  are prescribed, the vessel  $\Omega$  is described by an electric  $\pi$ -network, obtained as a cascade connection of a  $\mathcal{L}$ -network and a  $\mathcal{L}$ -inverted network (Fig. 10.9).

The four different representations of the same vessel arise from four different possible assumptions about the data prescribed at the upstream and downstream sections. In other words, they can be considered as the lumped parameter simplifications of four different “boundary” values problems.

**Remark 10.2.1** *Alternative ways can be pursued for devising lumped parameter models. Among the most recent, we mention the one proposed in [359]*

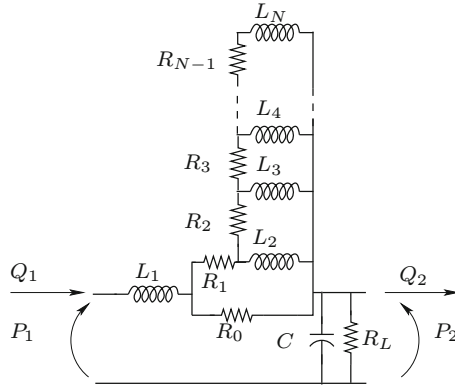


**Fig. 10.10.** Electric analog network of the Jager, Westerhof and Noordergraf model [244] including the sleeve effect and rheological effects. The larger  $N$  is, the more accurate is the model

which is based on suitable approximations of the inverse Laplace transform of the axisymmetric Stokes equations in rigid vessels.

Other lumped parameters models relying on more realistic assumptions have been proposed by different authors. For instance, we mention [244]. In this paper some modifications to the  $\mathcal{L}$ -inverted network of Fig. 10.7 (right) are proposed that account for the interactions between inertial and viscous phenomena induced by the pulsatility of blood flow (the so-called sleeve effect) and the non-Newtonian blood rheology (see Chapter 6). In particular, a boundary layer with lower viscosity due to the different concentrations of red cells is accounted for. The set up of the model was based on an explicit computation of the impedance associated to an approximation of the Womersley solution (see Chapter 5). The corresponding electric analog is depicted in Fig. 10.10. More accurate models can be obtained by including more elements, i.e. by taking higher values of  $N$ . Resistance  $R_0$  is related to the non-Newton effects, while  $R_L$  (where  $L$  stands for leakage) accounts for secondary vessels that are not accurately described in the model and however are relevant in the mass conservation.

The picture highlights the remarkably simple modifications to the lumped model required to account for the description of complex phenomena.

### 10.2.1 Lumped parameters models for the heart

As explained in Chapter 1, Section 1.1.1, the heart is subdivided into the right and the left parts, separated by the septum. The right heart supplies the pulmonary circulation, while the left one pumps the blood into the systemic tree. Each side consists of two chambers, the atrium and the ventricle, separated by the atrioventricular valves (the tricuspid valve in the right side, the mitral

valve in the left one). Their role is to receive fluid at low pressure and transfer it to a higher pressure region, acting as a *pump*. A possible representation of heart working is given by left ventricle pressure-volume diagrams (see [227] and Section 1.1).

Each ventricle can be described therefore as a vessel where the most significant feature is the compliance and *the compliance changes with time* (see [227, 256, 443, 509]).

The starting point for a candidate mathematical model is the relation that links internal pressure with the radius of an elastic spherical ball filled with fluid. Here and in the following we take  $P_{ext} = 0$ . We have

$$\pi R^2 P = 2\pi E h_0 R \frac{R - R_0}{R_0},$$

where  $R_0$  is the reference sphere radius (corresponding to  $P = 0$ ),  $h_0$  is a reference thickness of the ball surface and  $E$  denotes the Young's modulus. The contraction of the cardiac muscle may be taken into account by an increase of  $E$  (stiffening) and by a shortening of the muscle length (i.e. a reduction of  $R_0$ ). It is more convenient to express this relation as a function of the volume  $V$ , instead of the radius. By recalling that  $V = \frac{4}{3}\pi R^3$ , a linearisation procedure leads to

$$P = \frac{2E(t)h_0}{3R_0^2} \left(\frac{3}{4\pi}\right)^{1/3} V_0^{-\frac{2}{3}} (V - V_0),$$

where we have indicated the coefficients that change in time because of the action of the muscle. This simplified model does indeed describe the major characteristic of the ventricle. If we indicate  $C(t) = \frac{3R_0^2 V_0^{\frac{2}{3}}}{2E(t)h_0} \left(\frac{4\pi}{3}\right)^{1/3}$  we may re-write the relation in the more compact form

$$V(t) = C(t)P(t) + V_0(t).$$

By differentiating with respect to time we obtain

$$\frac{dV}{dt} = Q = \frac{dC}{dt}P + C\frac{dP}{dt} + M_Q(t), \quad (10.82)$$

where  $Q$  represents the (incoming) flow rate and  $M_Q = \frac{dV_0}{dt}$  is the action exerted by the contraction of the cardiac muscle.

A lumped representation (electric analog) of each ventricle<sup>2</sup> is given in Fig. 10.11, where  $R$  accounts for an additional viscous resistance inside the ventricle. Here,  $M_Q$  is represented by a current generator.

The electrical analog of the presence of heart valves has been represented in Fig. 10.11 by *diodes*. Ideally, the behaviour of a diode is described by the

<sup>2</sup> A mechanical representation of the heart working based on the classical Hill's model for the muscle can be found in [262] and [555].

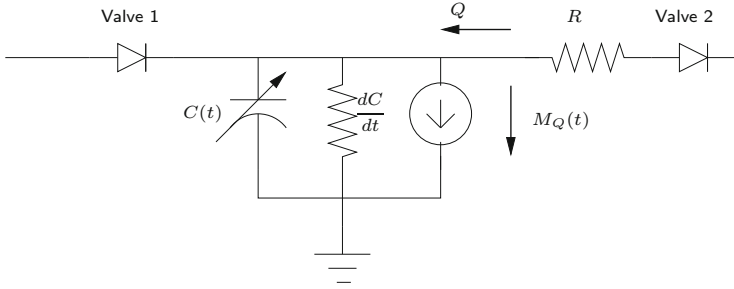


Fig. 10.11. Electric analog of the lumped parameter model of a ventricle

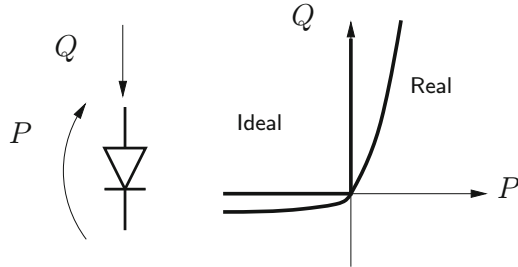


Fig. 10.12.  $P - Q$  curve in a diode, representing the electric analog of a heart valve

curve depicted in Fig. 10.12 and given by

$$\begin{aligned} P &= 0 & \text{if } Q > 0, \\ Q &= 0 & \text{if } P < 0. \end{aligned}$$

This means that the diode representation does not allow flow through the valve if the pressure is higher downstream than upstream. If the upstream pressure is higher, the diode allows the flow without any pressure loss. This is an “ideal” behaviour. Real valves have a different behaviour that can be represented by the curve

$$Q = Q_S (e^{\alpha P} - 1) \tag{10.83}$$

called *Shockley equation*. In some cases, this equation has been approximated by a piecewise polynomial curve (see e.g. [328]).

The presence of diodes introduces a nonlinear term in the system. However, if we resort to the Shockley model, the nonlinear terms are smooth in terms of mathematical regularity.

### 10.2.2 Lumped parameters models for the circulatory system

In the previous sections we have introduced lumped parameter description of two basic compartments, a segment of vessel and the heart. A possible model for the vascular network can be derived by “connecting” these compartments

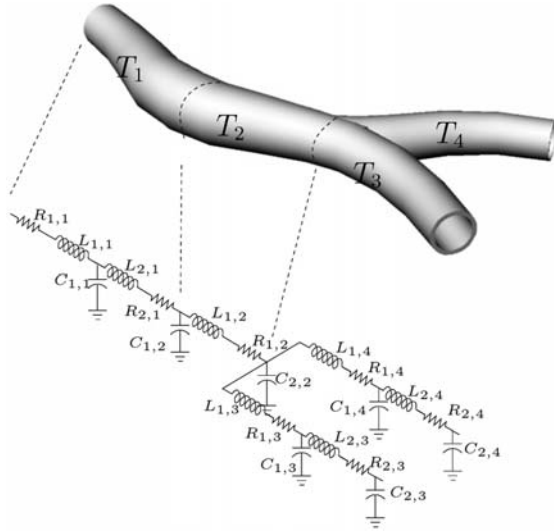


**Fig. 10.13.** Lumped parameters model for a branched vessel as a cascade of  $T$  and  $\pi$  networks

by means of appropriate *matching conditions*, in a way similar to the one pursued for the 1D model of bifurcations in Section 10.1.7. Matching conditions will be actually driven by *continuity of flux* and *balance of momentum* at the interfaces. More precisely, since our lumped parameter models deal with the flow rate  $Q$  and the pressure  $P$ , matching conditions will essentially state the continuity of these variables at the interfaces. In the electric analog, these relations correspond to the application of the classical *Kirchhoff laws* for the nodes (conservation of current/flow rate) and the nets (conservation of the voltage/pressure). For these reasons, lumped parameter models will also be referred to as *Kirchhoff* (K) models.

A sketch of possible connections of different compartments is given in Fig. 10.13.

More detailed models for the circulation are proposed in [353, 539], where hundreds of elementary compartments are considered.

### Mathematical and numerical analysis of lumped parameters models

From the mathematical viewpoint, a general representation of lumped parameters models is a system of differential-algebraic equations (DAE) of the form

$$\begin{aligned} \frac{dy}{dt} &= \mathbf{b}(\mathbf{y}, \mathbf{z}, t), \quad t \in (0, T], \\ G(\mathbf{y}, \mathbf{z}) &= 0, \end{aligned} \tag{10.84}$$

together with the *initial condition vector*  $\mathbf{y}|_{t=t_0} = \mathbf{y}_0$ . Here,  $\mathbf{y}$  is the vector of state variables, the vector  $\mathbf{z}$  contains the other variables of the network and  $G$  represents the algebraic equations derived from the Kirchhoff laws. Differentiating the algebraic equations with respect to time we get

$$\frac{dG(\mathbf{y}, \mathbf{z})}{dt} = \mathbf{J}_y \frac{d\mathbf{y}}{dt} + \mathbf{J}_z \frac{d\mathbf{z}}{dt} = 0$$

where  $\mathbf{J}_y = \frac{\partial G}{\partial \mathbf{y}}$  and  $\mathbf{J}_z = \frac{\partial G}{\partial \mathbf{z}}$  are the Jacobian matrices with respect to  $\mathbf{y}$  and  $\mathbf{z}$ . Assuming that  $\mathbf{J}_z$  is non singular, the DAE system is said to be of *index 1* (see e.g. [184]). This is the most frequent case in problems concerning lumped parameters models of the vascular system. We can then write

$$\frac{d\mathbf{z}}{dt} = -\mathbf{J}_z^{-1} \mathbf{J}_y \frac{d\mathbf{y}}{dt} = -\mathbf{J}_z^{-1} \mathbf{J}_y \mathbf{b}(\mathbf{y}, \mathbf{z}, t). \quad (10.85)$$

Assuming that an initial vector  $\mathbf{z}_0$  is available, the first equation of (10.84) and (10.85) can be rewritten as the classical Cauchy problem

$$\begin{aligned} \frac{d\mathbf{w}}{dt} &= \mathbf{a}(\mathbf{w}, t), \quad t \in (0, T], \\ \mathbf{w}(t_0) &= \mathbf{w}_0, \end{aligned} \quad (10.86)$$

where  $\mathbf{w} = [\mathbf{y}, \mathbf{z}]^T$  and  $\mathbf{a} = [\mathbf{b}, -\mathbf{J}_z^{-1} \mathbf{J}_y \mathbf{b}]^T$ . For the analysis of this problem we can refer to classical mathematical results, e.g. [214]. We will recall the following results:

1. if  $\mathbf{a}(\mathbf{w}, t)$  is continuously differentiable there exists a time interval  $[0, T^*]$  in which the solution of the problem exists and is unique;
2. if, moreover, the derivatives  $\partial \mathbf{a}_i / \partial w_j$  are bounded in the time interval  $[0, T]$ , then the solution of the Cauchy problem exists and is unique in  $[0, T]$ .

Numerical solution of Cauchy problems like (10.86) is an important branch of scientific computing. A general introduction can be found in [268]. Some basic ideas have been given in Section 2.3 in Chapter 2 for the Cauchy problems arising from the space discretisation of unsteady partial differential equations. Beyond the schemes mentioned there, we quote here a class of methods particularly useful for the problems considered here, namely the *Runge-Kutta methods*. Like the Euler and Crank-Nicolson methods, these schemes involve at each time step only the solution of the current and the previous steps, yielding however high accuracy by a splitting of the computation into an appropriate number of stages. These schemes can be explicit or implicit. For instance, the following is an explicit method of order 2 (called *Heun scheme*) given by

$$\begin{aligned} \mathbf{w}^* &= \mathbf{w}^n + \Delta t \mathbf{a}(\mathbf{w}^n, t^n), \\ \mathbf{w}^{n+1} &= \mathbf{w}^n + \frac{\Delta t}{2} (\mathbf{a}(\mathbf{w}^n, t^n) + \mathbf{a}(\mathbf{w}^*, t^{n+1})). \end{aligned}$$

Some Runge-Kutta methods have interesting practical features prone to *time adaptive implementations*. This means that with these methods it is possible to devise competitive a posteriori error estimators that can be used for adapting the time step to the solution dynamics. This feature is particularly useful in vascular problems where a fast transient (*systole*) is followed by a relatively steady phase (*diastole*). Furthermore, implicit Runge-Kutta schemes can be successfully used in *stiff problems*, i.e. problems where different components of the solution  $\mathbf{w}$  have so different dynamics that the fulfillment of stability and accuracy requirements could ask for an intensive computational effort (see e.g. [455]). These kind of problems can arise for instance when the lumped parameter representation of the vascular system couples a precise description of a district of interest with a rough description of the rest of the system. Other stiff problems arise when the dynamics of blood solutes (see the next section) is included in the mathematical model.

When the DAE problem (10.84) is of index higher than one, which is not the usual situation in this kind of problems, both the mathematical and numerical analyses become more involved. We refer the interested readers to [14, 184].

### 10.2.3 Lumped parameter models for modelling terminal vessels

By using the electrical analogy presented above, we now consider briefly some possible model for the terminal vessels to be used as stand-alone models or for computing boundary conditions to 1D networks (Section 10.1.5).

*Pure resistive load:* In some cases, the dynamics of blood in peripheral vessels is adequately represented by a simple algebraic law, see Fig. 10.14(right), given by

$$p(t) = RQ(t), \tag{10.87}$$

corresponding to the impedance  $Z_T(t - \tau) = R\delta(\tau - t)$ , where  $\delta$  denotes the Dirac delta. This is particularly true for small vessels where the heart pulsatil-

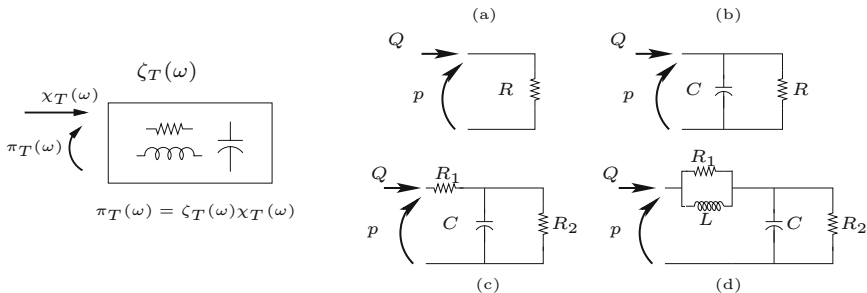


**Fig. 10.14.** Left: Terminal impedance for the peripheral circulation. Right: Lumped parameters representation (electrical networks) of possible impedances: (a) pure resistive load; (b) original windkessel model; (c) three elements windkessel; (d) four elements windkessel

ity has been almost completely attenuated by the larger vessel compliance and the motion is almost steady. An effective way of including this condition into the 1D model is based on the introduction of a *reflection coefficient*.

The reflection coefficient,  $R_t$ , is defined in [290] as the ratio of the magnitude of change of pressure across the reflected wave,  $\delta P$ , to the magnitude of change of pressure in the incident wave,  $\Delta P$ . By an appropriate linearisation and assuming that the pressure in the venous system is zero, it has been found that this ratio can be expressed as function of the terminal resistance at the vessel outflow and is related to the resistance  $R$  by the expression

$$R_t = \frac{\delta P}{\Delta P} = \frac{A_0 R - \rho c_0}{A_0 R + \rho c_0} = \frac{R - \rho c_0/A_0}{R + \rho c_0/A_0}.$$

The suffix 0 indicates the at rest state, i.e.  $Q = 0$  and  $A = A_0$ .

The value of  $R_t$  may vary between a free outflow when  $R_t = 0$  and a blockage when  $R_t = 1$ . The use of this parameter to characterise wave reflections caused by peripheral vessels is described in [535]. An advantage of using  $R_t$  instead of  $R$  is that it is related to pressure data only.

There is another possible definition for the reflection coefficient which is more suitable for prescribing boundary conditions based on the characteristic variables. More precisely,  $R_c$  is defined as

$$R_c = -\frac{W_{inc} - W_{inc,0}}{W_{out} - W_{out,0}},$$

where  $W_{inc}$  and  $W_{out}$  are the incoming and the outgoing characteristic variables at the boundary point, respectively. The negative sign is necessary to have a positive coefficient under normal conditions. A zero value of  $R_c$  indicates a perfectly non-reflecting boundary: the incoming characteristic variable is kept constant and equal to the value at rest, while  $R_c = 1$  is again associated to a perfect blockage (indeed, it can be verified that in this case  $u = 0$ ).

If we consider the right boundary  $x = x_2$  and use (10.87) we have the following expressions

$$W_{out} = W_1 = \frac{p}{RA} + 4c \quad \text{and} \quad W_{inc} = W_2 = \frac{p}{RA} - 4c.$$

Thus, if the rest value of the pressure is taken equal to 0, we have

$$R_c = -\frac{W_2 - W_{2,0}}{W_1 - W_{1,0}} = \frac{R_0 - p/4A(c - c_0)}{R + p/4A(c - c_0)}.$$

Using equations (10.39) and (10.87) it can be shown that  $R_c \simeq R_t$  and indeed we have an equality by linearising  $c$  around the rest configuration. At the numerical level,  $W_1$  can be computed for instance by extrapolation along the characteristic curves, refer to equation (10.46), the condition

$$W_2 = W_{2,0} - R_c(W_1 - W_{1,0}), \tag{10.88}$$

thus readily yields a boundary value for  $W_2$ .

*Windkessel models:* A more accurate representation of the terminal load is provided by the models including some possible dynamics related to vessel compliance and blood inertia. The first model was introduced by Otto Frank in 1899 [170]. It included a peripheral resistance and a compliance (see Fig. 10.14(b)) which yields a value of the impedance

$$\zeta_T(\omega) = \frac{R}{1 + \sqrt{-1}\omega RC}.$$

This model has been called *Windkessel* in analogy with the device (made of a reservoir and an air chamber) converting the alternate (periodic) water pumping of firemen into a steady flow. In order to better fit the experimental results (see [350, 539]), this basic model has been successively refined by Westerhof and his co-workers with the introduction of a second resistance (see Fig. 10.14(c)). The model has been called a *three-element Windkessel* or also familiarly *Westkessel*, and corresponds to an impedance value of

$$\zeta_T(\omega) = \frac{R_1 + R_2 + \sqrt{-1}\omega R_1 R_2 C}{1 + \sqrt{-1}\omega R_2 C}.$$

More recently (see [53, 483]), it has been pointed out that the fitting of experimental data with the three elements Windkessel model requires values that are not clearly related to the physical properties of the arteries. A new improvement of the model has been therefore proposed, leading to a four-element network (Fig. 10.14 right, (d)) that includes an inductor for inertial effects. The impedance of the model is

$$\zeta_T(\omega) = \frac{R_1 R_2 - C R_1 R_2 L \omega^2 + \sqrt{\omega}(R_1 + R_2)}{R_1 - C R_2 L \omega^2 + \sqrt{\omega}(L + C R_1 R_2)}.$$

The determination of an appropriate estimate of the parameters of these models is a difficult problem. The interested reader is referred to [53, 350, 483]. An intuitive and systematic approach to estimate the parameters of a three-element model is presented in [5].

The moduli of impedances and angles of the four networks considered in Fig. 10.14 are drawn in Fig. 10.15.

**Remark 10.2.2** *For including this kind of conditions in the 1D model, an alternative to equation (10.44) consists in formulating a condition in the time-domain for the Riemann variables (see the previous remark). For instance, by setting  $R = R_1 + R_2$ , the three-element Windkessel model corresponds to the boundary condition*

$$R_2 C \frac{R_a + R_1}{R_a + R} \frac{dW_2}{dt} + W_2 = R_2 C \frac{R_a - R_1}{R_a + R} \frac{dW_1}{dt} - R_c W_1,$$

that generalises (10.88) (see [158]).

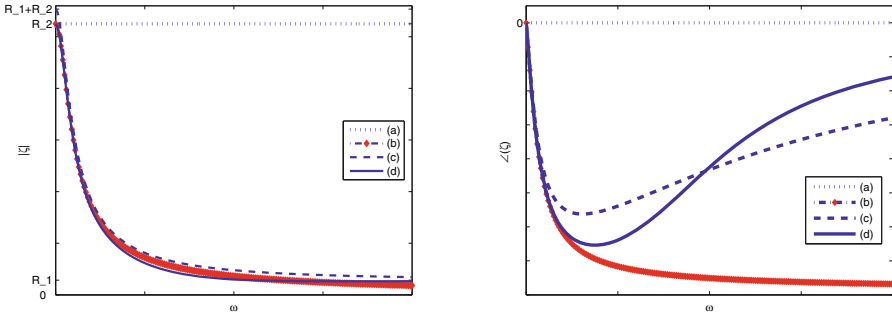


**Fig. 10.15.** Modulus (left) and angle (right) for the transfer function of the four networks in Fig. 10.14 (right)

*Structured tree model:* The dynamics spanned by family of Windkessel models is quite crude and in particular the wave propagation in the peripheral circulation is not well represented. A possible way for accounting these effects is the introduction of lumped parameters models with many elements, following the *geometrical multiscale approach* discussed in Chapter 11. A different approach, still resorting to the definition of an appropriate impedance function has been introduced in [358] and it is based on the representation of the terminal vessels as a structured tree (see Fig. 10.16).

By classical arguments in the wave theory (see e.g. [373]), the impedance at the beginning of a vessel with length  $l$  can be written as a function of the

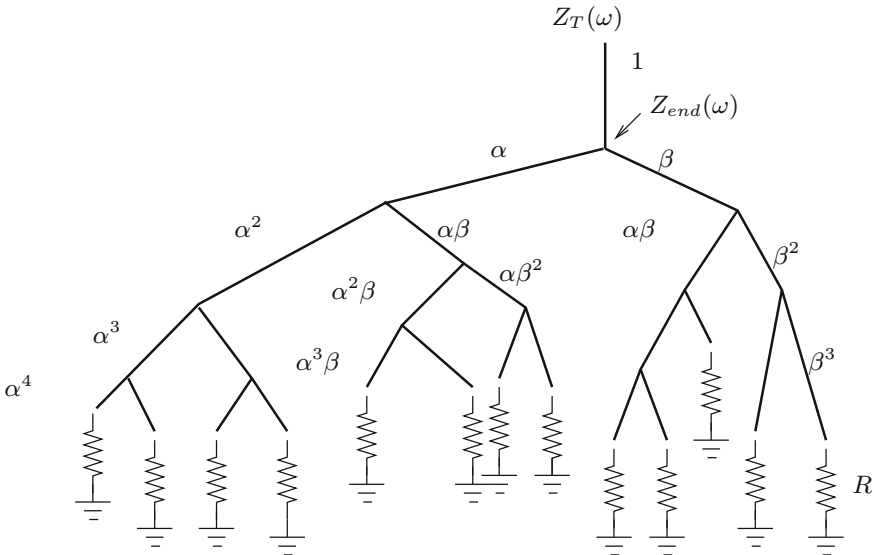


**Fig. 10.16.** Structured asymmetric tree representation of peripheral circulation

impedance at the end:

$$\zeta_{beg}(\omega) = \frac{g^{-1}\sqrt{-1}\sin(\omega l/c) + \zeta_{end}(\omega)\cos(\omega l/c)}{\cos(\omega l/c) + g\sqrt{-1}\zeta_{end}(\omega)\sin(\omega l/c)}, \quad (10.89)$$

where

$$g = A_0 \sqrt{\frac{3\sqrt{A_0}K}{2E\pi h\rho}}, \quad c = \sqrt{\frac{2E\pi hK}{3\sqrt{A_0}\rho}},$$

and  $K$  is an appropriate function of the Womersley number. The basic idea of this peripheral model is therefore to apply this formula for the terminal impedance  $\zeta_T$  that is expressed in this way as a function of the impedance at the end of the first peripheral vessel. The latter will be computed recursively by:

1. giving a model for the bifurcations in terms of impedance of parent and daughters vessels;
2. applying (10.89) for each branch of the vascular tree.

Continuity of pressure and flow rate at the bifurcation yields the condition linking the impedance of the parent vessel to the impedances of the daughter vessels (we assume branching with only two daughters)

$$\zeta_{parent} = \left( \frac{1}{\zeta_{d1}} + \frac{1}{\zeta_{d2}} \right)^{-1}.$$

Each branch of the tree is then scaled on the basis of the following assumptions:

1. at each bifurcation, the daughters branches scale asymmetrically with respect to the parent one with radius factors  $\alpha, \beta$  that can be determined on the basis of optimal branching considerations (see [358]);
2. under a certain threshold on the radius it is possible to assume that the impedance is purely a resistive load, known by experimental data.

Observe that the threshold is applied to the vessel radii and not to the number of branchings, so the number of branches is in general a function of the position of the interface with the 1D model and will be not assumed to be known a priori.

A more detailed code for this impedance modelling can be found in [364]. Results presented in [360] show that this approach for terminal outflow boundary conditions provide reliable results. In particular, it provides a closer physiological behaviour than the Windkessel models, with a correct phase-lag between flow and pressure.

See also [477] for an advanced application of this approach.

### 10.2.4 Modelling the interaction between cardiovascular system and chemical species

In the previous sections we have assumed that the parameters of the models depend on the morphological features and are *constant in time* (see equation (10.76)). This is a strong simplification since daily experience indicates that these parameters change in different physiological situations. Heavy exercise requires a body's response that involves biochemical reactions, chemicals transport (oxygen in particular) and definitely adjustments in blood flow. The cardiovascular system has feedback mechanisms that regulate its working activity and are essential for life (see e.g. [227]). The dynamics underlying these phenomena is extremely heterogeneous and complex, involving different chemical species, the cardiovascular and the nervous systems from peripheral to central districts (see [364], Chapter 7). There are *long-term* mechanisms that are essentially driven by the renal activity. Presence of water and salt or hormones can be adjusted by the kidneys for controlling arterial pressure. Other mechanisms belong to the *short term regulation effects*. In the latter case, the *central nervous system* (CNS) is the main mediator, involving *baroreceptors*, *mechanoreceptors* and *chemoreceptors*. The latter are sensitive to chemicals in blood (see Section 10.1.3). When the oxygen concentration drops, chemoreceptors increases cardiac strength and vasoconstriction. Baroreceptors are sensitive to the pressure alterations. They are located in the carotid sinus and the aortic arch. The role of the *baroreflex effect* is to keep the pressure within a physiological range. Mechanoreceptors are located in the atria and in the pulmonary veins and control arterial pressure by acting on the venous volume.

Other tuning dynamics are specifically present in the cardiovascular system. In particular, the *autoregulation* is a mechanism for maintaining an almost constant oxygen supply (in particular in the brain), driven by the smooth muscles in the vascular walls (see [2, 227]).

Lumped parameter models are an affordable mathematical and numerical tool for modelling these complex phenomena. Here we address some basic ideas for including feedback mechanisms in the models introduced so far. We essentially need:

1. lumped parameter models for chemical species, and
2. constitutive equations establishing the dependence of the parameters of the cardiovascular model on the concentration of chemicals.

We present these topics by means of an example based on Chapter 1 of reference [108].

#### Cardiovascular model

We assume the the cardiovascular system is represented by means of a set of four compartments (see Fig. 10.17):

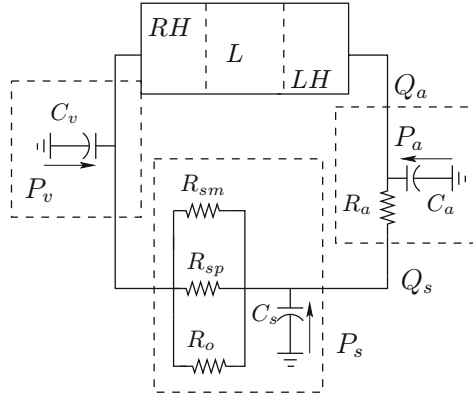


**Fig. 10.17.** Simplified compartment model of the circulation

*Right heart/lungs/left heart* acting as a forcing term for the whole system. *Large arteries* represented by a resistance  $R_a$  and a compliance  $C_a$ . *Systemic arteries* that are represented by the compliance  $C_s$  and three sub-districts:

1. *skeletal muscle* represented by the resistance  $R_{sm}$  and with flow rate  $Q_{sm}$ ;
2. *splanchnic compartment* with resistance  $R_{sp}$  and flow rate  $Q_{sp}$ ;
3. *other organs* with resistance  $R_o$  and flow rate  $Q_o$ .

The total systemic resistance will be given by

$$R_s = (R_{sm}^{-1} + R_{sp}^{-1} + R_o^{-1})^{-1}.$$

*Venous system* that is represented by the compliance  $C_v$  as their deformability is the more relevant feature of the veins.

The cardiovascular system will be therefore modelled by a lumped parameter model of the form

$$\begin{aligned} C_a \frac{dP_a}{dt} &= Q_a - \frac{P_a - P_s}{R_a}, \\ C_s \frac{dP_s}{dt} &= \frac{P_a - P_s}{R_a} - \frac{P_s - P_v}{R_s}, \\ C_v \frac{dP_v}{dt} &= Q_a - C_a \frac{dP_a}{dt} - C_s \frac{dP_s}{dt}, \\ Q_{sm} &= \frac{P_s - P_v}{R_{sm}}, \quad Q_{sp} = \frac{P_s - P_v}{R_{sp}}, \quad Q_o = \frac{P_s - P_v}{R_o}. \end{aligned} \tag{10.90}$$

Here  $Q_a$  is driven by the heart activity that can be simply given by

$$\begin{aligned} Q_a &= \frac{V_{str}}{T}, \\ V_{str} &= V_{ed}(P_v) - V_{u,vent} - \frac{P_a}{E}. \end{aligned} \quad (10.91)$$

Here,  $T$  is the *heart period*,  $V_{str}$  is the stroke volume of the heart. The latter is assumed to be a function of the end-of-diastole volume  $V_{ed}$ , which is in turn a function of the venous pressure  $P_v$ , of the (constant) unstressed ventricular volume  $V_{u,vent}$  and of the arterial pressure  $P_a$  by means of the heart *elastance*  $+E$ .

### Chemical model

Let us start considering only the dynamics of oxygen. We denote by  $[O_2]_i$  the oxygen concentration in compartment  $i$  ( $i \in (a, v, sm, sp, o)$ ) and by  $V_i$  is the volume of the  $i$  compartment. A possible law for the dynamics of oxygen in the systemic compartments ( $i = sm, sp, o$ ) is

$$V_i \frac{d[O_2]_i}{dt} = -r_i([O_2]_i, t) + Q_i(t) ([O_2]_a - \sigma_i [O_2]_i), \quad (10.92)$$

where  $r_i$  is the oxygen consumption rate and  $\sigma_i$  is a partition (constant) coefficient, function of the oxygen concentration in the different compartments *at rest*. The first term on the right-hand side is driven by the chemical reactions, while the second one is related to the *transport* associated to the blood flow. In the arterial compartment it is reasonable to assume that the oxygen consumption is negligible, so that  $[O_2]_a$  is constant. In the venous compartment, by mass conservation, we collect the residual oxygen coming from the systemic compartments and its concentration is thus given by

$$[O_2]_v = \sum_{i=sm,sp,o} \frac{Q_i}{Q_a} \sigma_i [O_2]_i.$$

A possible generalisation of this equation to the multi-chemical case is the following. We introduce a *vector* of chemical concentration  $\mathbf{c}_i$  so that  $c_{ki}$  is the concentration of the  $k^{th}$  species in compartment  $i$ . This model is given by

$$\begin{aligned} V_i \frac{d\mathbf{c}_i}{dt} &= A\boldsymbol{\psi}_i(\mathbf{c}_i, t) + \mathbf{b}_i(\mathbf{c}_a, \mathbf{c}_i, Q_i, t), \quad i = sm, sp, o, \\ \mathbf{c}_v &= \sum_{i=sm,sp,o} \frac{Q_i}{Q_a} S_i \mathbf{c}_i, \\ \mathbf{c}_a &= \mathbf{c}_a(\mathbf{c}_a^0, \mathbf{c}_v), \end{aligned} \quad (10.93)$$

where  $S_i$  is a diagonal matrix with entries given by the partition coefficients  $\sigma_{ki}$  and  $\mathbf{c}_a^0$  is the arterial vector concentration at rest. Moreover,  $\boldsymbol{\psi}_i$  is the vector of

consumption rates associated to chemical reactions and  $A_i$  is the so-called *stoichiometric matrix* representing the weighed connection of the species involved in the chemical reactions. Term  $\mathbf{b}_i$  represents the convection contribution to the chemical dynamics, driven by the blood flow. It is worth pointing out that since chemical reactions can have different time scales associated with each reaction, differential systems like (10.93) can in practice be *stiff*.

**Feedback model**

The dependence of chemical dynamics on fluid dynamics is clearly defined in the transport term  $\mathbf{b}_i$  of equation (10.93). Let us consider now how the chemical dynamics can affect the blood flow (see Fig. 10.18). To this aim, following [516], we introduce some new unknowns:

- $f_{es}$  represents the *efferent sympathetic activity*;
- $f_{ev}$  is the *efferent vagal activity*;
- $f_{cs}$  is the *carotid sinus firing rate*, that is the action generated by pressure alterations at the level of the carotid sinus;
- $f_{cm}$  is the *chemoreflex activity*;
- $\tilde{R}_i$  with  $i = sm, sp, o$  the state variables determining the systemic resistances and influenced by the vagal activity;
- $x_i$  with  $i = sm, sp, o$  the state variables determining the systemic resistances and influenced by the chemoreflex activity;
- $P_n$  a reference pressure value.

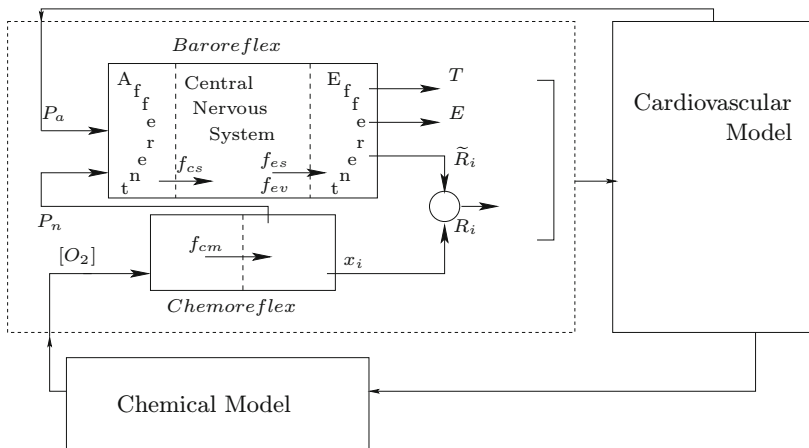


**Fig. 10.18.** Three compartments representation of the feedback cardiovascular model

We assume that the heart period  $T$  and the elastance  $E$  are influenced by the efferent vagal and sympathetic activities. In particular, we assume that

$$\begin{aligned}
 \frac{dT}{dt} &= \frac{1}{\tau_T} (T_0 - T - \sigma_{T,s}(f_{es}) - \sigma_{T,v}(f_{ev})), \\
 \frac{dE}{dt} &= \frac{1}{\tau_E} (E_0 - E - \sigma_{T,s}(f_{es})), \\
 f_{es} &= f_{es,\infty} + (f_{es,0} - f_{es,\infty}) \exp(-k_{es} f_{cs}), \\
 f_{ev} &= \frac{f_{ev,0} + f_{ev,\infty} \exp((f_{cs} - f_{cs,0})/k_{ev})}{1 + \exp((f_{cs} - f_{cs,0})/k_{ev})}, \\
 f_{cs} &= \frac{f_{\min} + f_{\max} \exp((P_a - P_n)/k_a)}{1 + \exp((P_a - P_n)/k_a)}.
 \end{aligned} \tag{10.94}$$

where  $\sigma$ ,  $E_0$ ,  $T_0$ ,  $f_{\infty}$ ,  $f_0$ ,  $f_{\min}$ ,  $f_{\max}$  and  $k$  (with their respective indices) represent appropriate functions and constants. The reference pressure  $P_n$  is driven by the chemoreflex activity and its temporal variation is given by

$$\frac{dP_n}{dt} = \frac{1}{\tau_{P_n}} (P_{n,0} - P_n - \sigma_{P_n,cm}(f_{cm})). \tag{10.95}$$

The systemic resistances are influenced both by the baroreflex and chemoreflex activities. More precisely, for  $i = sm, sp, o$  we have

$$\begin{aligned}
 \frac{d\tilde{R}_i}{dt} &= \frac{1}{\tau_{\tilde{R}_i}} \left( \tilde{R}_{i,0} - \tilde{R}_i - \sigma_{\tilde{R}_i,s}(f_{es}) \right), \\
 \frac{dx_i}{dt} &= \frac{1}{\tau_{x_i}} (x_{i,0} - x_i - \sigma_{x_i,cm}(f_{cm})),
 \end{aligned} \tag{10.96}$$

where finally we “assemble” the resistances

$$\begin{aligned}
 R_{sm} &= \frac{\tilde{R}_{sm}}{1 + x_{sm}}, \\
 R_{sp} &= \tilde{R}_{sp}(1 + x_{sp}), \\
 R_o &= \frac{\tilde{R}_o}{1 + x_o}.
 \end{aligned} \tag{10.97}$$

Finally, the chemoreflex control is driven by the oxygen concentration:

$$f_{cm} = \begin{cases} 0 & \text{if } [O_2]_{sm} > [O_2]_{sm}^0, \\ k_{cm} ([O_2]_{sm} - [O_2]_{sm}^0)^2 & \text{otherwise.} \end{cases} \tag{10.98}$$

Equations (10.90), . . . (10.98) represent a possible simplified model of feedback mechanisms in the cardiovascular system. More details can be found in [108, 363, 515, 516].

A major concern in the devise of this kind of models is the parameter identification based on experimental data. There are different approaches for pursuing this aim. Basically, the problem is recast into the form of the minimisation of the distance between an experimental data set and the corresponding results predicted by the theory, by acting on the values of the parameters to be estimated. The “optimal values” can be found by means of:

- *line search algorithms* (see e.g. [403]), that are quite cheap and however can found local (i.e. non global) optimal values;
- *genetic algorithms*, that compute the global optimal solution, even if with a larger computational cost. See [109] for more details.

### 10.3 Conclusions

Although this Chapter is limited to a basic introduction to simplified models of the circulatory system, we should stress that these models represent an important tool for quantitative cardiovascular investigations. The simple representation of a single vessel or a compartment makes these models well suited for an affordable description of complex dynamics among different vessels or compartments. As a matter of fact, in practice these models have been used in *cardiovascular mathematics* before the Navier-Stokes based models, because the latter require so many complex numerical techniques (and computational time) for providing quantitative results. In particular, 1D models are appropriate for describing pressure wave propagation along the vascular tree [316], and at which extent this can be affected by some pathologies, prostheses or aging [3, 4, 158]. Lumped parameter models, on the other hand, are extremely useful for describing complex dynamics among compartments, in particular when the space details are not so relevant, like in the case of estimation of blood flow reserves in some compartment (usually the coronary reserve) or the feedback mechanisms.

The main drawback of these models is the loss of some details that could be relevant at the systemic level, despite of their local nature. For this problem, a possible approach is to couple together local and systemic models, as it is addressed in the next chapter.